Estimation of groundwater recharge in a shallow sandy aquifer using unsaturated zone modeling and water table fluctuation method

Anna Gumuła-Kawęcka [a], Beata Jaworska-Szulc [a], Adam Szymkiewicz [a,*], Wioletta Gorczewska-Langner [a], Małgorzata Pruszkowska-Caceres [a], Rafael Angulo-Jaramillo [b], Jirka Šimůnek [c]

[a] *Gdańsk University of Technology, Faculty of Civil and Environmental Engineering, Gdańsk, Poland*
[b] *Univ Lyon, Université Claude Bernard Lyon 1, CNRS, ENTPE, UMR 5023 LEHNA, F-69518 Vaulx-en- Velin, France*
[c] *University of California Riverside, CA, USA*

ARTICLE INFO

ABSTRACT

Quantification of groundwater recharge is one of the most important issues in hydrogeology, especially in view of the ongoing changes in climate and land use. In this study, we use numerical models of 1D vertical flow in the vadose zone and the water table fluctuation (WTF) analysis to investigate local-scale recharge of a shallow sandy aquifer in the Brda outwash plain in northern Poland. We show that these two methods can be jointly used to improve confidence in recharge estimation. A set of preliminary numerical simulations based on soil water content measurements from 4 grassland and pine forest profiles provided a wide range of recharge estimates (263 mm to 839 mm for a 3-year period). Additional simulations were performed with the lower boundary condition specified as a functional relationship between the groundwater table elevation and the rate of groundwater outflow from the vertical profile (horizontal drains boundary condition). In this way, we could reproduce the water table fluctuations resulting from recharge and lateral discharge to nearby lakes. The agreement between simulated and observed groundwater levels differed depending on the specific set of parameters characterizing vadose zone flow, which allowed us to find the most representative parameter sets and refine the range of plausible recharge estimates (501 mm to 573 mm per 3 years). The recharge rates from WTF (410 mm to 606 mm per 3 years) were in good agreement with numerical simulations, providing that the effect of the natural recession of groundwater table due to lateral outflow was considered (master recession curve method). Our results show that: (i) the proposed approach combining 1D vadose zone modeling and WTF improves recharge estimation, (ii) multiple types of observations, including groundwater table positions, are needed to calibrate and validate vadose zone flow models, and (iii) extended periods of observations and simulations are necessary to capture year-to-year variability in the recharge rates.

1. Introduction

Sustainable management of groundwater resources requires an accurate estimation of groundwater recharge flux. This knowledge is essential to quantify the safe yield of an aquifer in the hydrological balance of catchment (Bouwer, 1989; de Vries & Simmers, 2002; Sophocleous, 1991). The groundwater recharge flux also plays a significant role in the transport of contaminants because it determines the travel time through the unsaturated zone (e.g., Sousa et al., 2013; Szymkiewicz et al., 2018b; 2019), contaminant load reaching the aquifer (e.g. Szymkiewicz et al., 2020), directions of groundwater flow

in shallow aquifers (e.g., Scanlon et al., 2002a), and consequently vulnerability of aquifers, and in particular groundwater intakes, to health-related hazards. This is particularly true for shallow, unconfined aquifers, such as aquifers located on outwash plains. An outwash plain, also named 'sandur', is mostly a sandy deposit formed by glacial ablation water. It is a geomorphological form widely occurring in the glacial landscape of the North European Plain, Fennoscandia, northern Siberia, Canada, and the northern US. A significant spatial extent and high hydraulic conductivity of the outwash deposits make sandurs abundant groundwater bodies commonly used to supply water.

Several studies have been carried out in recent years to quantify

---

groundwater recharge on outwash plains and other sandy deposits of similar character in temperate and cold climates. Their results are summarized in Table 1 in terms of the average annual recharge and the recharge/precipitation ratio ω. In colder areas, such as Finland, Sweden, and western Canada, where melting of snow and ice rapidly reaches groundwater (Şen, 2015), recharge can reach almost 70% of the yearly precipitation. In warmer and more humid regions, recharge is usually lower because of less snow and longer vegetation period, which increase evapotranspiration (ET). Groundwater recharge in the North European Plain (e.g., Poland or western Russia), with a more continental climate (precipitation 500 – 700 mm/yr), is about 9 – 24% of precipitation in forested or agricultural areas. In the lowlands with more abundant rainfall (greater than700 mm/yr), such as northern Germany, Belgium, or the eastern coast of North America, recharge ranges between 13 and 34% of precipitation in agricultural areas, 24 – 51% in coniferous forests, and 28 – 53% in grasslands.

A variety of methods is used to estimate groundwater recharge. They can be broadly categorized as physical techniques, water-budget methods, numerical modeling, and tracer methods (Healy, 2010; Scanlon et al., 2002a). Within these groups, we can distinguish methods based on measurements from different hydrological compartments, i.e., the unsaturated zone, the saturated zone, and surface water. Using several methods is recommended to obtain reliable results (Healy, 2010; Lerner et al., 1990; Scanlon et al., 2002a; Simmers, 1997). In the studies of Callahan et al. (2012), Huet et al. (2016), Jie et al. (2011), Krogulec (2010), Liu et al. (2014), Szilagyi et al. (2011), and Zomlot et al. (2015), recharge estimations in temperate climate were conducted with at least two methods.

Numerical models of vadose zone flow are increasingly applied to obtain recharge estimates, including most of the studies reported in

Table 1. Unsaturated zone models can be based on the solution of the Richards equation (e.g., HYDRUS-1D (Šimůnek et al., 2013)), the kinematic wave equation (e.g., MODFLOW UZF (Niswonger et al., 2006)), or soil water balance equations (e.g., WETSPASS (Batelaan & De Smedt, 2001) and HELP (Schroeder et al., 1994)). The required computer programs are often freely available. They can represent a number of factors influencing recharge in a physically based manner, which makes them an ideal tool for capturing the variability of recharge in space and time and for investigating scenarios of land use or climate change. However, such models require a significant number of parameters that may be difficult to obtain. Consequently, the resulting recharge estimates are prone to uncertainties resulting from (a) spatial variability of soil (e.g., layering), (b) uncertainty in the water retention and hydraulic conductivity functions, and (c) uncertainty in parameters determining root water uptake and ET (e.g., leaf area index LAI and root depth). In order to provide a meaningful prediction of recharge, vadose zone models must be calibrated and validated against field measurements and other methods of recharge estimation (Jie et al., 2011). This is not a simple task since data on vadose zone flow and ET are difficult to obtain. Moreover, including this data in the calibration process does not guarantee that a unique set of model parameters is derived. Brunner et al. (2012) showed that at least in some scenarios using ET data in calibration constrains the vadose zone model better than soil moisture measurements, while the most valuable input for model calibration is represented by groundwater heads. Jie et al. (2011) proposed an approach to cross-validate recharge rates from the soil water balance model using observations of groundwater table fluctuations. They calculated specific yield based on the recharge estimate from the soil model and the increment of groundwater table observed in the corresponding time period. The obtained values of specific yield were

Table 1
Groundwater recharge based on selected studies of unconfined sandy aquifers.

Reference	Location	Land cover	Applied method	Precipitation [mm/yr]	Recharge [mm/yr]	Recharge/ Precipitation ratio ω [-]
Cherkauer & Ansari (2005)	Southeastern Wisconsin, USA	Agricultural, urbanized	Baseflow analysis	989	224–248	0.23–0.25
Nastev et al. (2005)	Southwestern Quebec, Canada	Agricultural, urbanized	Water table fluctuations	930–1130	131–225	0.13–0.22[1]
Smerdon et al. (2008)	Northern Alberta, Canada	Boreal forest	Numerical modeling (in-house code)	410	45	0.11
Wendland et al. (2008)	Lower Saxony, Germany	Mixed crops and pasture	Numerical modeling (GROWA)	740	150–250[2]	0.20–0.34
Dripps & Bradbury (2010)	Northern Wisconsin, USA	Grass Coniferous forest	Soil – water balance model	570–980	160–435 140–425	0.28–0.53 0.24–0.51
Krogulec (2010)	Vistula River valley, central Poland	Forest-agricultural	Groundwater model (MODFLOW) Water table fluctuations	589	56–95 75	0.10–0.16 0.13
Grinevskii & Novoselova (2011)	Moscow Artesian Basin, western Russia	Forest Field	Unsaturated flow model (HYDRUS-1D)	657 667	138 100	0.21 0.15
Leterme & Mallants (2011)	Dessel, Belgium	Coniferous forest	Unsaturated flow model (HYDRUS-1D)	899	239	0.27
Leterme et al., (2012)	Dessel, Belgium	Grass	Unsaturated flow model (HYDRUS 1D)	899	314	0.35
Kurylyk & MacQuarrie (2013)	New Brunswick, eastern Canada	Coniferous and deciduous forest	Soil-water balance model (HELP3)	1230	541(average)	0.44 (average)
Ala-aho et al. (2014)	Northern Finland	Pine forest	Numerical modeling (CoupModel)	591	363 (average)	0.61(average)
Graf & Przybyłek (2014)	Poznań Plateau, western Poland	Forest	Soil-water balance model (WetSpass)	517–579 541 (average)	46–13181 (average)	0.09–0.24 0.15 (average)
Wu (2014)	Tärnsjö, central Sweden	Coniferous forests	Unsaturated flow model (CoupModel)	600	210–310	0.35–0.52
Pozdniakov et al. (2015)	Voronezh, southwestern Russia	Forest	Unsaturated flow model (HYDRUS-1D)	558–672	130	0.19–0.23
Åberg et al. (2019)	Northern Finland	Forest	Groundwater model (MODFLOW)	560	315–378	0.56–0.68

[1] compared to the average precipitation of 1030 mm/yr.
[2] locally more than 250 mm/yr.

compared to the expected values for the aquifer to check if the measured water table fluctuations are consistent with the simulated recharge episodes.

Groundwater level measurements are simpler to perform and usually more available than vadose zone data or ET measurements. However, including them in a state-of-the-art 1D vertical model of vadose zone flow based on Richards' equation is not straightforward, as it is related to the choice of the boundary condition (BC) at the bottom of the soil column. In vadose zone flow simulations, the bottom BC is often formulated in terms of the water pressure head corresponding to the measured position of the water table, which can be constant or variable in time. If the water table elevation varies rapidly in time, using it as the BC can lead to unphysical water fluxes at the bottom of the unsaturated zone, which causes errors in recharge estimations (Beegum et al., 2018). Moreover, using a pressure head-based BC does not allow reproducing the natural sequence of water table fluctuations resulting from infiltration and ET processes occurring in the vadose zone. Alternatively, the bottom of the soil column can be assumed impermeable (Brunner et al., 2012). In this case, one can represent water table fluctuations due to vadose zone processes, but the influence of lateral groundwater flow is neglected, which is unrealistic for many aquifers, especially those discharging to nearby surface water bodies. The third option is the free drainage boundary condition, where the bottom of the soil column is above the groundwater table, and outflow is driven by gravity, with the vertical pressure head gradient equal to zero (e.g., He et al., 2021; Healy, 2010; Ines & Mohanty, 2008; Šimůnek et al., 2013; Zendehboudi et al., 2012). The bottom flux gives an estimate of recharge, but the exact arrival time of recharge at the water table cannot be reproduced, and information about water table elevation is not included in the model.

In this study, we suggest using yet another option for the bottom BC in vadose zone simulations, i.e., the pressure head-dependent flux. The bottom of the soil profile is below the groundwater table, and the outflow rate from the saturated zone is calculated as a function of the current water table position. The function contains two parameters, which are calibrated using the observed water table levels. The calibration procedure can be performed for different sets of vadose zone and ET parameters to find which parameters allow for the best agreement between the observed and calculated water table fluctuations. In this way, uncertainty related to the estimation of vadose zone parameters and the resulting recharge rates is reduced.

Besides their utility for the calibration and validation of vadose zone flow models, groundwater level observations in shallow unconfined aquifers can be used to estimate recharge by the water table fluctuation method (WTF) (Healy, 2010; Scanlon et al., 2002a). This method requires only one parameter – the specific yield S_y. Unfortunately, S_y is difficult to determine, as it depends on the type of soil, the depth to the groundwater table, and water dynamics in the vadose zone (Healy, 2010). The simplest variant of WTF is the RISE method (Rutledge, unpublished manuscript, after Delin et al., 2007), which assumes that recharge events only occur when there is an increase in the groundwater level. The RISE method tends to underestimate recharge. In reality, the changes in the groundwater level are driven by other processes besides recharge and ET, especially lateral flow towards streams, lakes, and other surface water bodies. Thus, recharge also often occurs when the water table is stagnant or decreases, but this is masked by lateral outflow. In order to account for this factor, the MRC method has been proposed (Heppner & Nimmo, 2005, Delin et al., 2007; Heppner et al., 2007, Jie et al., 2011). In this approach, a master recession curve (MRC) is identified for a specific observation well using observations from dry periods. MRC represents a decrease in the groundwater level due to lateral outflow and other discharge processes in the absence of recharge. The rate of the water table decline ($\Delta H/\Delta t$) decreases with a decreasing water table elevation H, and several approaches have been proposed to establish a functional relationship between these two quantities (Nimmo et al., 2015). The water level increments are calculated with respect to the MRC, leading to higher recharge estimates than using the RISE

method (Delin et al., 2007). Thus, the results of the WTF analysis are affected by uncertainty related to the choice between the RISE and MRC methods, the estimation of MRC, and specific yield.

The aim of our study was to combine vadose zone flow modeling based on the Richards equation with pressure head-dependent flux as the bottom BC and the WTF analysis, in order to reduce the uncertainty in recharge estimation. The two methods are applied to local-scale recharge estimates on the experimental site on the Brda outwash plain in northern Poland. Another objective was to assess time variability of the recharge in a 3-year observation period, which contained an extremely wet year, followed by an extremely dry year. The influence of land cover (grassland vs. pine forest) and the related estimates of LAI and root depth on groundwater recharge were also investigated.

2. Study area

Field measurements were carried out on a site near Tuchola town in northern Poland. This area is a part of the Brda sandur, considered to be the largest outwash plain in Poland. The experimental site is almost completely surrounded by four lakes (Fig. 1). The land is covered mainly by pine forests, with some open grasslands, crop fields, and dispersed
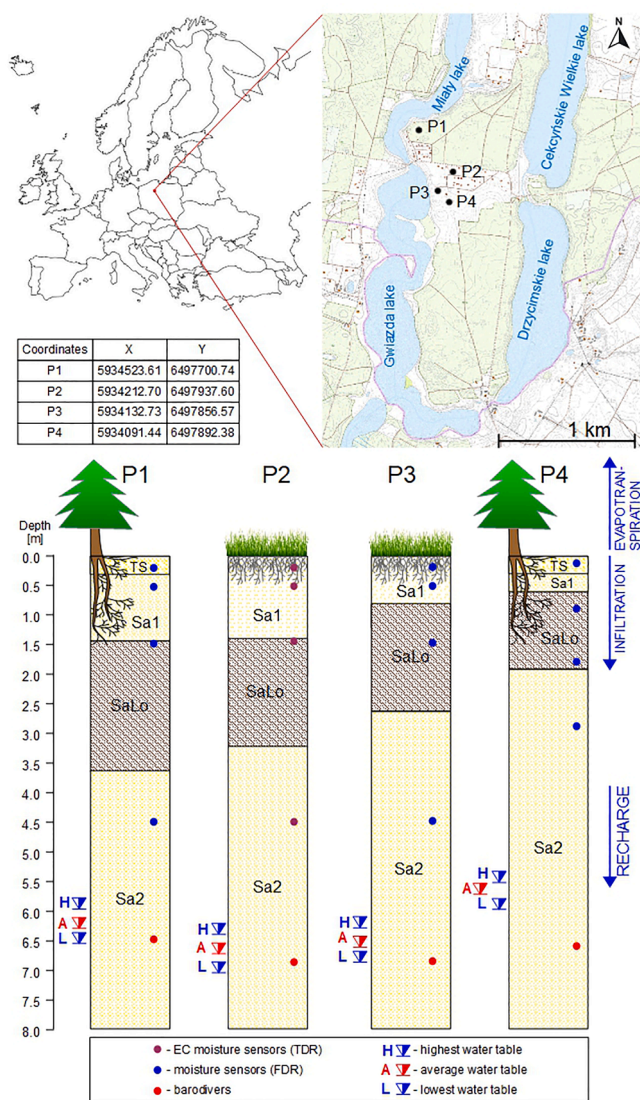

Fig. 1. Location of the observation site and soil profiles (modified from Gumuła-Kawęcka et al., 2018). H, L and A denote the highest, the lowest and the average elevation of the water table in the 3-year observation period.

low buildings (summer houses and farms). According to the data from the weather station in Chojnice (35 km from the experimental site) for the period 1951–2019, the yearly average air temperature in the region is 7.4 °C, and the average annual precipitation is 581 mm.

Figure 1 presents the soil profiles obtained from 4 observation boreholes (P1 and P4 in pine forest, P2 and P3 on grassland). In each profile, we can distinguish two sand layers (Sa1 and Sa2), separated by a loamy sand / sandy loam layer (SaLo), occurring about 1.5 m below the ground level and 1.5 to 2 m thick. Moreover, in P1 and P4, we distinguished a layer of topsoil (TS) based on the observed differences in soil water dynamics with respect to Sa1. Below the vadose zone is a shallow aquifer, with the water table at a depth of 6 to 7 m and the bottom at a depth of about 15 m. The aquifer is composed of fine/medium sand with gravel. It is recharged by infiltrating precipitation and drained by surrounding lakes which are connected to Brda river with a stream. Below the shallow aquifer is a layer of weakly permeable glacial till (15 to 24 m below ground level (b.g.l.), not shown in the profiles), which overlies a deeper, confined aquifer. The lower aquifer, also composed of glacio-fluvial sand with gravel, is recharged by the upper aquifer, which was confirmed by Oficjalska and Gregosiewicz (2000) and Muter (2002). Measurements performed in another borehole in October 2016 showed that the piezometric level in the deeper aquifer was about 0.6 m below the groundwater table in the shallow aquifer, which corresponds to a vertical hydraulic gradient of 0.095.

There is a regional tendency of lowering groundwater tables in shallow unconfined aquifers within the Brda outwash plain (Jaworska-Szulc et al., 2017). The analysis of groundwater levels in 10 monitoring wells for the period of 2003–2016, obtained from the monitoring network, showed a long-term trend of water table lowering since 1990. In most cases, the groundwater table has been below the monthly average water level since 2006. The tendency is related to lower infiltration recharge, likely caused by climate change (less snow cover, irregular and more intensive rainfall events in summer). The lowering of the water table in the shallow aquifer may reduce or eliminate the recharge gradient between the shallow and deeper aquifers, which could be a long-term and potentially irreversible effect. Preliminary numerical simulations of vadose zone flow based on literature data (Gumuła-Kawęcka et al., 2018) showed significant year-to-year variability of groundwater recharge, following changes in annual precipitation in the period 2003–2016. Regional-scale estimations of average annual groundwater recharge in the Brda river watershed (from baseflow measurements) were given by Hobot et al. (2012). They range from 155 mm/yr for the upper part of the watershed (above Tuchola) to 193 mm/yr for the whole watershed, which corresponds to 26% and 33% of the average precipitation in Chojnice, respectively.

3. Methods

3.1. Field measurements of hydrological data

Continuous soil and groundwater data measurements were carried out from April 15, 2017, to April 14, 2020, in 4 observation profiles (P1-P4). The water table level and the electric conductivity of groundwater were recorded using sensors (baro-divers Decagon Devices CTD-10) placed in piezometers, screened in the interval of approximately 5 to 11 m below the ground level (b.g.l.) in each piezometer. Volumetric water content was measured in each profile using automatic sensors (TDR, Decagon Devices, GS3 and FDR, Delta_T Devices SM150) at four depths (ranging from 20 cm to 450 cm b.g.l., Fig. 1).

Meteorological data (precipitation, temperature, air pressure, relative humidity, wind speed and direction, and solar radiation) was collected by a weather station located in an open field (P2) from April 15, 2017, to July 30, 2019. An additional pluviometer was placed in the forest (P1) to estimate interception. All measurements of weather, soil, and groundwater data were recorded by automatic data loggers in 10-minute intervals.

3.2. Soil hydraulic characteristics

Several methods were applied to estimate hydraulic characteristics for soils at the site. They included pedotransfer functions based on particle soil distribution, single ring infiltrometer tests, tension infiltrometer tests, saturated hydraulic conductivity measurements with the Aardvark permeameter (SoilMoisture Equipment Corp.), and measurements of soil water retention functions with sand-kaolinite apparatus. A detailed presentation of the results is outside the scope of this report and will be the subject of a separate study. Here we use data derived from field measurements to constrain calibration of vadose zone flow models.

We assumed that each soil layer is homogeneous and isotropic within each specific profile, but parameters of the same layer may differ between profiles. Hydraulic characteristics of soils were described with the van Genuchten-Mualem model (van Genuchten, 1980):

$$S_e = \frac{\theta - \theta_r}{\theta_s - \theta_r} = \left[1 + (\alpha|h|)^{n_g} \right]^{-m_g} \tag{1a}$$

$$K = K_s K_r = K_s S_e^\tau \left[1 - \left(1 - S_e^{1/m_g} \right)^{m_g} \right]^2 \tag{1b}$$

where S_e is the effective saturation [-], θ_r is the residual volumetric water content, θ_s is the saturated volumetric water content, α is the parameter related to the average pore size [L^{-1}], n_g, m_g are parameters related to the pore size distribution [-], $m_g = 1–1/n_g$, K is the unsaturated hydraulic conductivity [LT^{-1}], K_s is the saturated hydraulic conductivity [LT^{-1}], K_r is the relative hydraulic conductivity [-] and τ is a parameter related to pore geometry [-].

The saturated water contents θ_s for the TS, Sa1, and SaLo layers were set equal to the average porosity, as measured on undisturbed soil samples. Since no undisturbed samples were taken from Sa2, we assumed that it is more compact due to the self-weight of the soil and set $\theta_s = 0.35$, which was the minimum value measured in the upper layer Sa1. The residual water contents θ_r were set to be slightly below the smallest values measured by soil moisture probes in the TS, Sa1, and Sa2 layers, while in SaLo, we set it to 0.057 (an average value for loamy sand, according to Carsel and Parrish (1988)). The saturated hydraulic conductivities K_s for the TS and Sa1 layers were obtained from single ring infiltrometer tests and measurements with the Aardvark permeameter and from permeameter measurements and pumping tests for the Sa2 layer.

Pumping tests were conducted in piezometers to determine the horizontal hydraulic conductivity of the aquifer. Wells were pumped with a constant rate of about 4.6 m³/h. The water level was measured in 15-minute intervals until drawdown stabilized. Hydraulic conductivity was calculated based on the Dupuit method with the Forchheimer correction for partial penetration. The radius of drawdown was estimated using the Kusakin empirical formula (Pazdro & Kozerski, 1990). Due to these simplifying assumptions, the calculated hydraulic conductivity must be considered as approximate. Nevertheless, it is in good agreement with the measurements using the Aardvark permeameter in the same sand layer Sa2, about 1.5–2 m above the water table. The pore connectivity parameter τ was set to the default value of 0.5 in all soil layers, except Sa2 in P1, where τ was calibrated, to ensure better agreement between field measurements of water content and simulations. The remaining parameters, i.e., α and n for all layers and K_s for SaLo, were found by calibration of the numerical model described below. Permeameter measurements of K_s for the SaLo layer were not included in the calibration due to the large variability of results and potential errors.

3.3. Numerical simulations with a constant water table

Numerical models of vadose zone flow were developed for each profile using the HYDRUS-1D computer program (Šimůnek et al., 2013). HYDRUS-1D solves the Richards equation describing vertical flow in a

variably-saturated soil profile.

$$\frac{\partial \theta(h)}{\partial t} = \frac{\partial}{\partial z}\left(K(h)\frac{\partial h}{\partial z}\right) + \frac{\partial k(h)}{\partial z} - S(h) \qquad (2)$$

where θ is the volumetric water content [L^3L^{-3}], t is time [T], h is the water pressure head (negative in the unsaturated zone), z is the spatial coordinate [L], $K(h)$ is the hydraulic conductivity function of the unsaturated medium [LT^{-1}], and $S(h)$ is a sink function representing water uptake by plant roots [$L^3L^{-3}T^{-1}$].

For spatial discretization of Eq. (4), HYDRUS-1D uses Galerkin-type linear finite elements with mass lumping, while a fully implicit first-order scheme is used for time discretization. Further details about the numerical scheme can be found in the code documentation (Šimůnek et al., 2013). The code has been validated in a large number of applications (Šimůnek et al., 2008; 2016), many of them related to the estimation of groundwater recharge (e.g., Batalha et al., 2018; Grinevskii & Novoselova, 2011; Leterme et al., 2012; Leterme & Mallants, 2011; Pozdniakov et al., 2015; Scanlon et al., 2002b; Šimůnek et al., 2016; Szymkiewicz et al., 2018a; Twarakavi et al., 2008).

Two series of simulations were carried out. In the first series, the profile depth was set to the average depth to groundwater table measured in the observation period (as shown in Fig. 1), and the bottom boundary condition was given as $h = 0 = const$. These simulations were used to calibrate the models and estimate groundwater recharge. We used uniform spatial discretization with 1 cm node spacing. In order to avoid the influence of the initial condition on the results, we applied a 3-year warm-up period, starting with the water pressure distribution close to field capacity and using weather data from the Chojnice station.

An atmospheric boundary condition was specified on the soil surface using precipitation and potential evapotranspiration fluxes. No water ponding was assumed to occur at the soil surface (instantaneous runoff), and the minimum allowed pressure head on the soil surface in dry periods (separating stage 1 from stage 2 of evaporation) was set to −1000 m. We used precipitation measured by rain gauge at P2 (grassland) in the main simulation period from April 15, 2017, to April 14, 2020, and measurements from the Chojnice weather station in the warm-up period (April 15, 2014 – April 14, 2017). Interception was included according to the model implemented in HYDRUS-1D, based on von Hoyningen-Hüne (1983), Braden (1985), and van Dam et al. (1997).

$$I = a \cdot \text{LAI}\left(1 - \frac{1}{1 + \frac{P \cdot \text{SCF}}{a \cdot \text{LAI}}}\right) \qquad (3)$$

where I is interception [LT^{-1}], a is the interception constant [LT^{-1}], LAI is leaf area index [-], P is precipitation [LT^{-1}], SCF is the soil cover fraction [-], estimated as SCF = 1-exp(-0.463·LAI). The interception constant a was set to 0.25 mm for grassland (a typical value for crops) and 0.37 mm for the forest. The latter value ensured the best agreement between the interception calculated in the HYDRUS model and the interception measured on-site (difference in precipitation recorded by gauges on the open field and in the forest).

Potential evapotranspiration (PET) was calculated with the Penman-Monteith equation (Allen et al., 1998), as implemented in Hydrus-1D, using daily weather data measured at the site (2017–20) and in Chojnice (2014–17). When calculating PET, we used a typical range of LAI based on Scurlock et al. (2001). The average LAI in temperate evergreen needle leaf forests is 5.47, with a standard deviation of 3.37. Since pine forests in Poland tend to have sparse canopies (Jagodziński & Kałucka, 2008), we took LAI = 2.10 and 5.47 as our site's lower and upper estimates, respectively. For grasslands, Scurlock et al. (2001) reports average LAI = 1.71 (+/-1.19). As the area has a relatively dense grass cover, we took LAI = 1.71 and 2.90 as the upper and lower estimates, respectively. LAI was assumed constant throughout the year since both types of plant cover are perennial, and winters in the simulated period

were relatively mild (see section 4.1 and Table 2). For the same reason, we did not consider soil freezing (preliminary simulations showed that the difference in recharge estimates with and without soil freezing is negligible). According to de Beer's law, PET was divided into the potential evaporation flux at the soil surface and potential transpiration in the root zone (Šimůnek et al., 2013). We assumed nonlinear root distribution with depth, according to Jackson et al. (1996):

$$Y = 1 - \beta^d \qquad (4)$$

where Y is the cumulative root fraction (from 0 to 1), $\beta = 0.943$ for grassland (P2 and P3) or 0.976 for temperate coniferous forest (P1 and P4), and d is a depth in cm. The resulting root density sharply decreases with depth, which is consistent with the fact that even in pine forests, the majority of roots typically occur within the uppermost 20 cm of the soil, and only very few roots can be found below 1.5 m (Rutkowski et al. 2017; Sainju & Good, 1993). Root water uptake of grass and pine forest was estimated with the Feddes et al. (1978) macroscopic model. The plant-specific stress response function parameters were taken from De Silva et al. (2008).

For each observation profile, we simulated two scenarios using the lower and upper estimates of LAI. In each scenario, the soil parameters not derived from field measurements were found using inverse modeling by fitting the numerical solution to measured water contents in each profile. Time series of daily-averaged water contents in 30-days intervals from all four depths (P1, P2, P4 – 20, 50, 150, 450 cm, and P3 – 10, 90, 180, 280 cm) were used for that purpose. The optimization of soil hydraulic parameters was carried out using the Marquardt-Levenberg algorithm implemented in HYDRUS-1D. The recharge estimate corresponding to the calibrated soil parameters was taken as the final result of the simulation in each scenario.

3.4. Numerical simulations with lateral groundwater outflow

The second series of simulations aimed to validate the numerical models described in the previous section by reproducing observed variations in groundwater table elevations. For each profile, we used the set of calibrated parameters from the earlier simulations. The only changes introduced in the second series of simulations were: (i) extending each profile to a depth of 8 m (keeping the same node spacing of 1 cm), to include the upper part of the aquifer in the Sa2 layer, and (ii) setting the bottom boundary condition to a relationship between the hydraulic head and flux, to represent lateral groundwater discharge to nearby lakes. For this purpose, we used the "Horizontal drains" feature of Hydrus-1D. The simplest analytical formula describing flow to drain available in Hydrus is a simplification of Hooghoudt's equation:

$$q_{dr} = \frac{4K_{dr}}{L_{dr}^2}(H - H_{dr})^2 = C(H - H_{dr})^2 \qquad (5)$$

where q_{dr} is the lateral outflow (discharge to drains) per unit area, K_{dr} is the horizontal hydraulic conductivity, L_{dr} is the drain spacing, H is the water table elevation in the soil profile, H_{dr} is the water table elevation in the drain, and $C=(4K_{dr}/L_{dr}^2)$ is a lumped parameter representing hydraulic conductance of the aquifer and aquifer/lake interface. Unfortunately, no detailed water level measurements in the lakes were performed, and it likely changed during the observation period. On the other hand, groundwater flow was influenced by factors not represented in Eq. (5), e.g., vertical hydraulic gradients or low permeability of the lake bottom sediments. In principle, it is possible to use more complex models instead of Eq. (5), but then more parameters need to be estimated or calibrated. For the sake of simplicity, we used Eq. (5) and considered H_{dr} and C as fitting parameters. Their values were estimated by manual calibration, based on the difference between the observed and calculated positions of the water table in each profile, calculated as the sum of square errors SSQ = $\Sigma (H_{obs} - H_{sim})^2$, where H_{obs} and H_{sim} are the observed and simulated elevations of the groundwater table.

Table 2
Climate data for the experimental site: (1) from Chojnice weather station, (2) measured on site.

Period	Average daily temperature [°C]	Potential evapotranspiration [mm/yr]		Annual precipitation [mm/yr]	Number of days with average temperature < 0 °C	Number of days with snow cover
		LAI = 1.71	LAI = 5.74			
15 April 2014–14 April 2015	9.3[1]	681.4	1034.6	507.7[1]	42[1]	24[1]
15 April 2015–14 April 2016	9.1[1]	725.0	1106.8	418.8[1]	36[1]	20[1]
15 April 2016–14 April 2017	8.8[1]	642.2	964.7	703.6[1]	51[1]	52[1]
15 April 2017–14 April 2018	8.2[2]	521.3	610.1	919.6[2]	54[2]	32[1]
15 April 2018–14 April 2019	10.2[2]	633.4	722.1	463.0[2]	42[2]	12[1]
15 April 2019–14 April 2020	10.1[2]	591.4	676.5	670.4[2]	9[2]	4[1]

HYDRUS-1D allows two options to incorporate the calculated flux q_{dr} in the discrete form of the Richards equation. It can be added to the bottom node as a boundary condition in the strict sense, or it can be distributed over all nodes below the groundwater table as a sink term. The latter option seemed more consistent physically with the assumption of horizontal groundwater flow and was used in our simulations.

3.5. Estimation of specific yield

We combined several approaches to derive a plausible range of specific yield values for our site, including literature data (Johnson, 1967, Healy, 2010) and the empirical formula of Bieciński (Pazdro & Kozerski, 1990) commonly used in Poland, which links S_y to the hydraulic conductivity of the aquifer K_s:

$$S_y = 0.117 \sqrt[7]{K_s} \qquad (6)$$

where Ks is given in [m/d]. In the above formula, we used the estimate of K_s in the Sa2 layer in each profile. Finally, we also estimated S_y from HYDRUS-1D simulations with a lateral outflow boundary condition. For each day of the simulation, we calculated the volume of water in the lower section of the profile, which contained fluctuating water table. The zone included in the calculations stretched from the bottom of the profile to some height above the water table, as discussed later. Assuming that the soil profile represents a column of 1 m² cross-section, we express the volume of water as the equivalent water height H_w in meters. The specific yield S_{yi} for a given day i was calculated as:

$$S_{yi} = \frac{\Delta H_{wi}}{\Delta H_i} \qquad (7)$$

where ΔH_{wi} is the daily change in water volume and ΔHi is the daily change in groundwater table position (both quantities can be either positive for increasing water table or negative for decreasing water table). The final value of S_y was obtained as an average of S_{yi} for all days of the simulation period. Due to transient effects, one can obtain S_{yi} negative or larger than soil porosity for some days. These values were excluded from the calculation of the average S_y.

Some consideration is needed to choose the upper limit of the zone affected by the water table fluctuations, which is the basis for calculating H_w. If the upper limit is too close to the water table, it is in the capillary zone, and the resulting S_y is very small. If it is too close to the soil surface, S_y is affected by surface infiltration and evapotranspiration, which are unrelated to water table fluctuations. A preliminary analysis for profile P1 showed that the results were relatively consistent if the upper limit of the calculation zone was set in the range from 1 m above the highest position of the water table in the profile to the bottom of the SaLo layer. Thus, we set the upper limit of the zone for calculating S_y 1 m above the highest position of the water table in each profile.

3.6. Water table fluctuation (WTF) analysis

The WTF analysis was based on water level measurements in piezometers, averaged for each day of the observation period. The daily amount of recharge R_i is calculated as:

$$R_i = S_y \Delta H_i \qquad (8)$$

where S_y is the specific yield and ΔH_i (greater than 0) is an increment in the groundwater table elevation caused by recharge occurring between day i-1 and i. A range of S_y values was obtained using the methods described in the previous section. We applied two methods (RISE and MRC) to calculate the increments ΔH_i. The RISE method assumes that recharge only occurs if there is an increase in groundwater table elevation between two subsequent days, so $\Delta H_i = H_i - H_{i-1}$ if $H_i > H_{i-1}$, otherwise $\Delta H_i = 0$.

The MRC method assumes that in the absence of recharge, the water table decreases daily by a specific amount ΔH_{MRCi}, following the so-called master recession curve (MRC), which represents in a simplified manner the discharge processes in the aquifer, in particular the lateral outflow to nearby surface water bodies.

The groundwater table tends to decrease at a rate depending on its current position, i.e., the higher the water table, the faster the lowering rate (Heppner & Nimmo, 2005). MRC provides a functional relationship between a daily decrement of the water table ΔH_{MRCi} and the water table elevation H_{i-1} in periods without recharge. In this study, we used the simplest, linear MRC:

$$\Delta H_{MRCi} = A \cdot H_{i-1} + B \qquad (9)$$

The coefficients A and B were fitted separately for each piezometer. The fit was based on data from periods of continuous groundwater level decrease longer than two weeks. More refined methods to estimate MRC are available (Heppner & Nimmo, 2005; Jie et al., 2011), but we considered the approach described here as sufficiently accurate for the purposes of our study. The daily increment of the water level due to recharge was then calculated as: $\Delta H_i = H_i - H_{i-1} + \Delta H_{MRCi}$ if $H_i > (H_{i-1} - \Delta H_{MRCi})$, otherwise $\Delta H_i = 0$ (the decrement ΔH_{MRCi} taken as a positive number).

4. Results and discussion

4.1. Weather data and measured groundwater levels

Figure 2 shows daily precipitation totals measured at the P2 observation point from April 15, 2017, to April 15, 2020. There is a significant
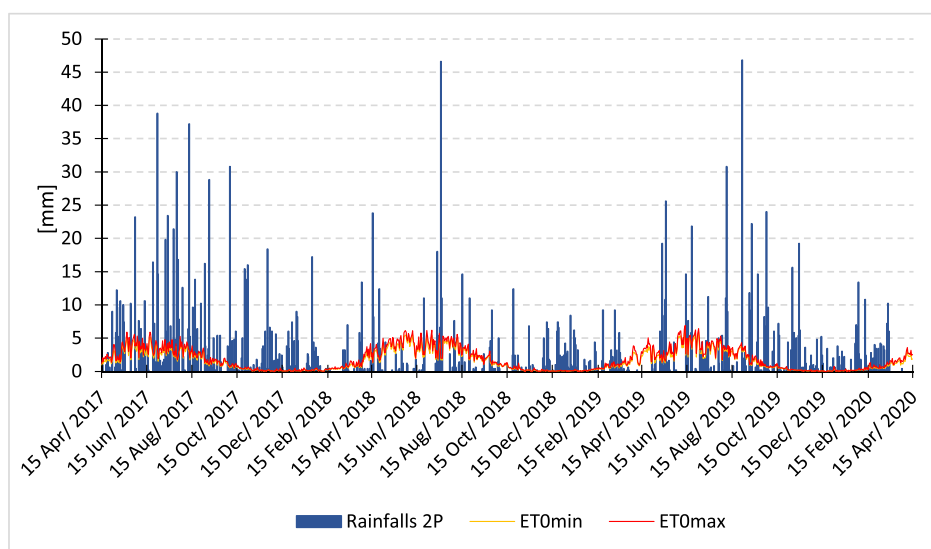
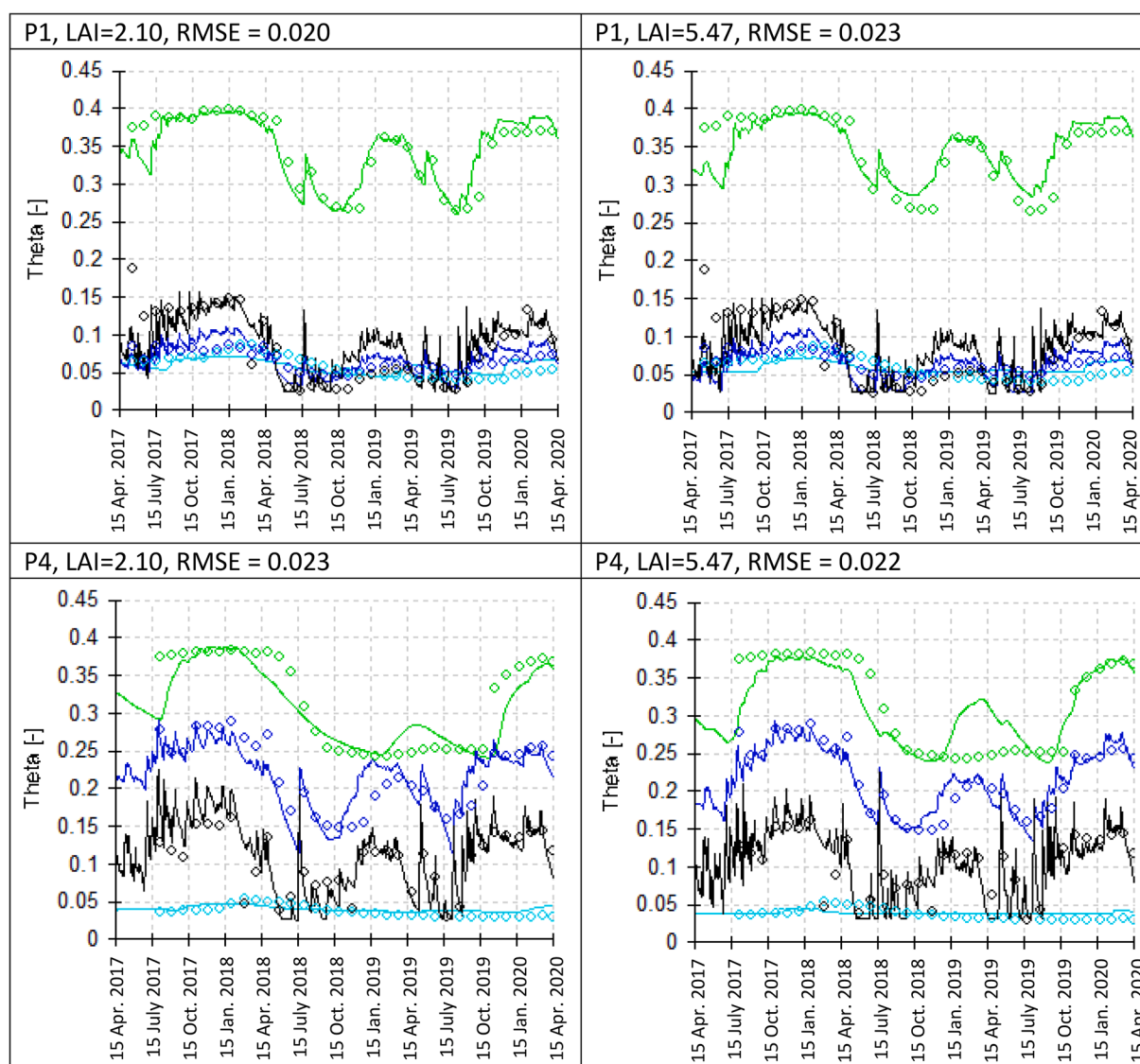**Fig. 2.** Precipitation and potential evapotranspiration at the observation site.

Fig. 3. Measured and simulated water contents in the forest profiles P1 and P4 (sensor depth: 20 cm (black), 50 cm (dark blue), 150 cm (green), 450 cm (light blue)).

difference between meteorological conditions during the three years of observation (Table 2). The one-year period starting on April 15, 2017, was exceptionally wet – the amount of precipitation measured by a rain gauge at profile P2 (open field) reached 920 mm (more than 150% of the long-term average), with a mean temperature equal to 8.2 °C. In contrast, the one-year period starting on April 15, 2018, was unusually warm and dry, with an average temperature of 10.2 °C and precipitation of 462 mm. The third year (April 15, 2019 – April 14, 2020) was warm (10.1 °C), but the rainfall total was slightly above average – 670.4 mm/y. Among the 36 months of the observation period, 32 months had monthly temperatures higher than the long-term average for the considered month, based on long-term (1951–2020) observation data from Chojnice station. Ten months in the observation period were extremely warm, within 5% of the warmest months in the years 1951–2020.

Yearly precipitation measured by the rain gauge in the forest (P1) was 687 mm in the first year, 321 mm in the second year, and 501 mm in the third year, indicating that average interception by the forest canopy was about 27% of yearly precipitation. This is compatible with the range observed in pine woods in Poland (Puchalski & Prusinkiewicz, 1990).

Maximum and minimum daily values of PET calculated with the Penman-Monteith equation are also presented in Fig. 2. The annual PET was the lowest in the first year (starting on April 15, 2017) – between 521.3 and 610.1 mm, while PET reached the highest values in the second year (April 15, 2018 –April 14, 2019) – from 633.4 mm to 722.1 mm. In the third year (starting on April 15, 2019), PET ranged between 591.4 mm and 676.5 mm. The differences are caused mainly by different weather conditions during vegetative periods in 2017, 2018, and 2019. In 2017, the vegetation period (May – October) was relatively cold and rainy, with an average temperature of 14.5 °C and a precipitation amount of 682 mm. In contrast, in 2018, the vegetative period was extraordinarily warm and dry, with an average temperature of about 16.5 °C and a rainfall total of 234 mm. More mild conditions were during the vegetation period in 2019 – the mean temperature reached 15.5 °C, but the precipitation sum was 438 mm.

The measured values of volumetric soil water content are presented in Figs. 3 and 4. A distinct pattern of seasonal variability can be seen, with wet periods: Apr 2017 - Apr 2018, Oct 2018-Apr 2019, Oct 2019-Apr 2020, and dry periods in Apr-Oct 2018 and Apr-Oct 2019. In the first year of observations, there is an exceptionally long wet period with high water contents at all sensors, which is not repeated in the subsequent drier years. Under the sandy loam layer, water content
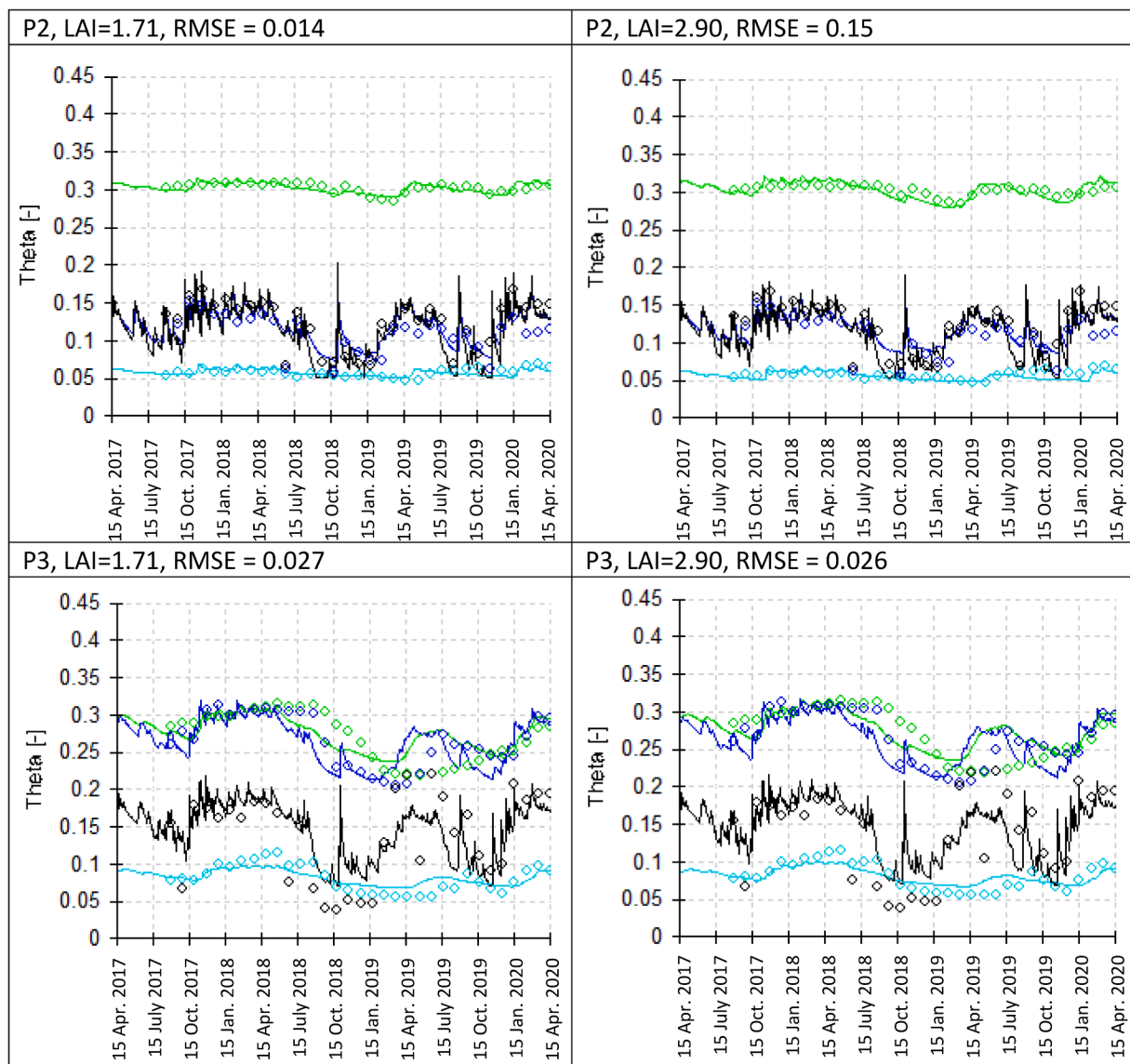

Fig. 4. Measured and simulated water contents in the grassland profiles P2 and P3 (sensor depth: 2P –20 cm (black), 50 cm (dark blue), 150 cm (green), 450 cm (light blue), and 3P – 10 cm (black), 90 cm (dark blue), 180 cm (green), 280 cm (light blue)).

fluctuations in the Sa2 layer are generally much smaller than in the TS and Sa1 layers. In the SaLo layer, the water content is significantly higher than in other layers due to finer soil texture. The fluctuations in this layer are larger in forest profiles than in grassland profiles, probably due to water uptake by deeper tree roots in dry periods.

A clear variability pattern can also be seen in water table elevations measured in four profiles (Fig. 5). In the first (wet) year, the groundwater table increased monotonically. Then it decreased, reaching the lowest elevation in September 2019, and rose again in the last months of the observations. During the long period of decline, we can distinguish an interval with a relatively low decline rate in autumn/winter 2018/19, corresponding to increased soil water contents in Figs. 3 and 4. In contrast, during the vegetation periods in 2018 and 2019 (Apr-Oct), we observe low soil water contents and a sharp groundwater table decline. There are some breaks in water table measurements in P1 and P2 due to malfunctions of the sensors. Also, the water table elevation in P2 is above the other three piezometers starting from mid-2018 which is probably caused by technical issues with the barodiver and the breaks in operation mentioned above. Different flow dynamics might have also played a role since P2 is the well farthest away from the lakes. Overall, the soil moisture and groundwater table show strong seasonal and year-to-year variability related to large differences in annual precipitation and ET.

4.2. Soil hydraulic characteristics and soil water contents

Parameters of the van Genuchten model for all profiles and soil layers are summarized in Table 3. The saturated hydraulic conductivity obtained from field measurements in the Sa1 and Sa2 layers does not differ substantially between the profiles, with K_s in Sa2 consistently higher than in Sa1. In P1 and P4, the topsoil is characterized by a lower hydraulic conductivity than the underlying Sa1 sand layer. In contrast, K_s

in the SaLo layer (obtained from inverse numerical solution) shows significant differences between profiles, with the lowest values in P1 and the highest in P2 (different by a factor of about 500). In most cases, the calibrated values of α and n were sensitive to the choice of LAI, which strongly influenced evapotranspiration. However, we obtained a similar fit quality in each of the eight scenarios, reported as RMSE in Table 2. In terms of RMSE, the best fit was obtained for P2, and this is confirmed by a visual comparison of simulated and measured water contents in Figs. 3 and 4. On the other hand, in P2, the pattern of water content evolution is different from other profiles since the water content is almost constant in the SaLo layer, while in other locations, it decreased significantly during the dry periods.

4.3. Recharge estimates from numerical simulations

Figure 6 shows annual and total (3-year) recharge values obtained using the simulations with a constant water table position and the final calibrated sets of parameters in each scenario. They differ significantly between the profiles and strongly depend on LAI, ranging from 263 mm in P4 with an LAI of 5.47 to 839 mm in P2 with an LAI of 1.71 in the three years. For the lower LAI estimates, recharge can be even more than two times larger than for the upper LAI estimate due to smaller interception and ET. There is a reasonable similarity in predictions for the two forest profiles (P1 and P4). There is no overlap in the results for the two grass profiles, with the lower estimate in P2 minimally exceeding the upper estimate in P3. In contrast, the range calculated for P3 partly overlaps with the estimates for P1 and P4.

There are also clear differences in the time distribution of the recharge flux arriving at the groundwater table. Four examples are shown in Fig. 7. In all cases, recharge occurs mostly during the initial (wet) year of the observations. However, in P1-LAI2.10 and P2-LAI2.90, the flux increases and later decreases gradually over longer time periods,
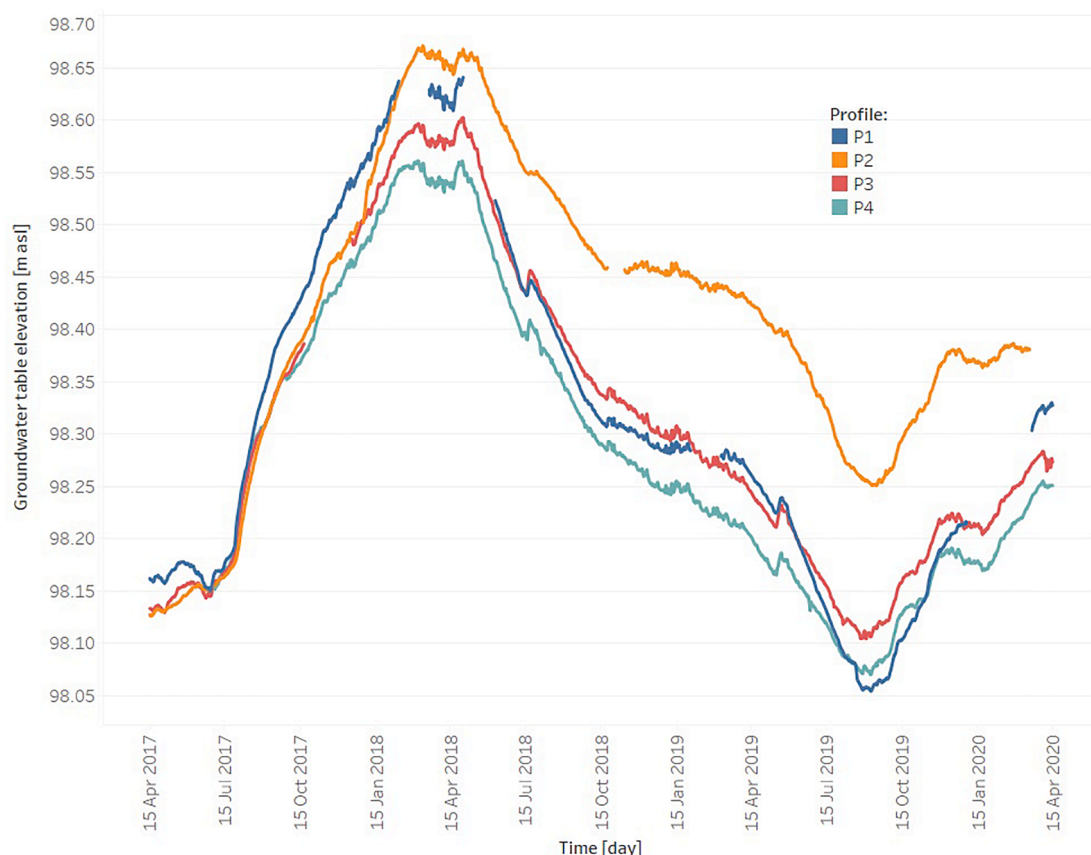

Fig. 5. Groundwater table elevation measured in piezometers at four observation sites.

Table 3

Parameters of the soil hydraulic functions (values obtained using inverse modeling are denoted by superscripts: 1 – simulations with a lower LAI estimate, 2 – simulations with an upper LAI estimate).

		P1	P2	P3	P4
Topsoil (TS)	θ_r [-]	0.025	n/a	n/a	0.025
	θ_s [-]	0.400			0.400
	K_s [cm/d]	238			91
	α [1/cm]	0.007[1,2]			0.018[1], 0.012[2]
	n [-]	2.76[1], 2.46[2]			2.20[1], 1.88[2]
	τ [-]	0.5			0.5
Sand (Sa1)	θ_r [-]	0.025	0.045	0.045	0.025
	θ_s [-]	0.400	0.400	0.400	0.400
	K_s [cm/d]	1356	813	506	502
	α [1/cm]	0.010[1,2]	0.037[1], 0.019[2]	0.014[1,2]	0.053[1], 0.017[2]
	n [-]	2.48[1], 2.32[2]	1.70[1], 1.74[2]	1.63[1], 1.62[2]	1.29[1,2]
	τ [-]	0.5	0.5	0.5	0.5
Sandy loam (SaLo)	θ_r [-]	0.057	0.057	0.057	0.057
	θ_s [-]	0.410	0.410	0.410	0.410
	K_s [cm/d]	0.2[1,2]	102[1], 107[2]	35[1], 33[2]	0.2[1], 2[2]
	α [1/cm]	0.002[1], 0.001[2]	0.004[1], 0.006[2]	0.009[1], 0.008[2]	0.005[1], 0.002[2]
	n [-]	3.61[1], 2.89[2]	1.80[1], 1.39[2]	1.38[1], 1.39[2]	4.00[1], 1.43[2]
	τ [-]	0.5	0.5	0.5	0.5
Sand Sa2	θ_r [-]	0.025	0.045	0.025	0.025
	θ_s [-]	0.350	0.350	0.350	0.350
	K_s [cm/d]	3737	3767	3145	4216
	α [1/cm]	0.015[1], 0.014[2]	0.038[1], 0.029[2]	0.037[1], 0.040[2]	0.036[1], 0.021[2]
	n [-]	3.53[1], 3.20[2]	3.45[1], 3.37[2]	1.89[1], 1.87[2]	2.99[1], 3.64[2]
	τ [-]	2.08[1], 1.97[2]	0.5	0.5	0.5
RMSE [-]		0.020[1], 0.022[2]	0.014[1], 0.015[2]	0.027[1], 0.026[2]	0.023[1], 0.022[2]

while in P2 and P4, separate recharge events are clearly marked as peak flux values. Moreover, in P2, relatively large fluxes occur in the second and third years of the observation period. In P1 and P3, there is only small recharge in the second year and somewhat larger recharge in the last year. Finally, in P4, there is practically no recharge in the second year and only a small flux in the last year. These results are consistent with the differences in soil hydraulic parameters and LAI between the simulations.

Considering the whole 3-year period of observations, the recharge/precipitation ratio varies from 13% to 41%, depending on the considered scenario. Note that despite such a wide variability, the R/P ratio falls within the range of values reported in Table 1. Since we obtained a reasonably good fit to the measured water content values in all cases, additional information was required to reduce the uncertainty resulting from the variability of soil characteristics and the lack of precise data on evapotranspiration. Thus, another series of simulations was carried out to reproduce the groundwater table's observed fluctuations and narrow the range of recharge predictions.

4.4. Water table fluctuations from numerical simulations

The water table fluctuations obtained using numerical simulations with a lower boundary condition representing lateral outflow are shown in Figs. 8 and 9. In each case, the best fit resulting from manual calibration of boundary condition parameters is presented. The results were found to be quite sensitive to both H_{dr} and C, which facilitated their calibration. H_{dr} determined the average elevation of the water table, while C influenced both the average elevation and amplitude of fluctuations (Fig. 10). However, the shape of the curve is determined by the distribution of recharge over time, and it is not fundamentally affected

by either H_{dr} or L_{dr}.

The agreement between the best fit and observations varied depending on the soil profile and LAI. The lowest SSQ values ($1.5 \cdot 10^4$) were obtained for P1 with an LAI of 2.10 and P3 with an LAI of 2.90. This is confirmed by a visual inspection of the plots, which shows a relatively good agreement between observations and the model for most of the simulation period. For P4 with an LAI of 2.10, the SSQ is only slightly larger ($1.6 \cdot 10^4$), but the fit is clearly worse for the rising branch of the hydrogram, corresponding to the initial wet period. The largest SSQ were obtained for P2, where the groundwater table measurements were probably inaccurate, as discussed earlier, while on the other hand, the recharge estimates were higher than for other profiles. For the forest profiles (P1 and P4), the fit was better for the lower LAI estimate (2.10), while for the grass profiles (P2 and P3), it was better for the higher LAI estimate (2.90). The results presented in Figs. 8 and 9 indicate that simulations for P1 and P4 with an LAI of 2.10 and P3 with an LAI of 2.90 provided recharge estimates, which are most representative for our sites, i.e., they are in the best agreement with the observed pattern of groundwater level fluctuations. Consequently, total recharge in the observed period can be estimated to be between 501 and 573 mm, a significantly narrower range than the one resulting from the first series of simulations. The corresponding LAI falls between 2.10 and 2.90, representing the upper estimates for grassland and lower estimates for pine forests.

The fitted values of conductance coefficient C fall in the range from $1.32 \cdot 10^{-5}$ to $4.44 \cdot 10^{-5}$ cm.d^{-1}. The corresponding theoretical distance between the observed profile and the lake (half of the drain spacing) can be calculated from Eq. (5), assuming the aquifer permeability $K_{dr} = 3716$ cm/d (an average value for the Sa2 layer from Table 2). The obtained distance is between 91 and 168 m. This is in reasonable agreement with the real distances: 30 m for P1, 170 m for P2, 70 m for P3, and 90 m for P4. Note, however, that there is no clear relationship between the fitted C value and the real distance to the lake at a specific point.

4.5. Estimation of specific yield

Healy (2010), following Johnson (1967), reports $S_y = 0.21$ for fine sands with the standard deviation +/- 0.07. Since K_s estimates for Sa2 are quite similar in each profile (Table 3), the empirical formula of Bieciński, Eq. (6), gives a narrow range of S_y estimates: 0.191 to 0.200. S_y derived from the second series of numerical simulations (with a fluctuating water table) ranged from 0.229 (P3, LAI = 1.71) to 0.300 (P4, LAI = 2.10), with an average of 0.269. These results are consistent with the upper range of estimates given by Healy (2010), which can be explained by the high uniformity of grain sizes in Sa2. Ultimately, in the WTF analysis, we used 0.200 and 0.280 as the lower and upper estimates of S_y for our sites.

4.6. Recharge estimations using WTF

The master recession curves for each profile are shown in Fig. 11. There is a considerable scatter between the points representing the relationship between the groundwater table elevation (H) and a daily decrement of the groundwater level (ΔH_{MRC}). In each case, it was possible to fit a linear trend, showing an expected decrease of the absolute value of ΔH_{MRC} with decreasing H, but the results must be considered as highly approximate.

Figure 12 presents groundwater table increments calculated using the RISE and MRC methods for P3. Both methods produce a similar pattern of recharge variability. However, in the MRC approach, there are significantly more days with recharge, and the estimated recharge rates are higher than in the RISE method. According to the MRC procedure, recharge also occurs when there is a decline in the groundwater table, but it is smaller than the decline resulting from the master recession curve. This can be seen especially in the period from Oct 2018 to Apr 2019, characterized by a small decrease in the groundwater table, as
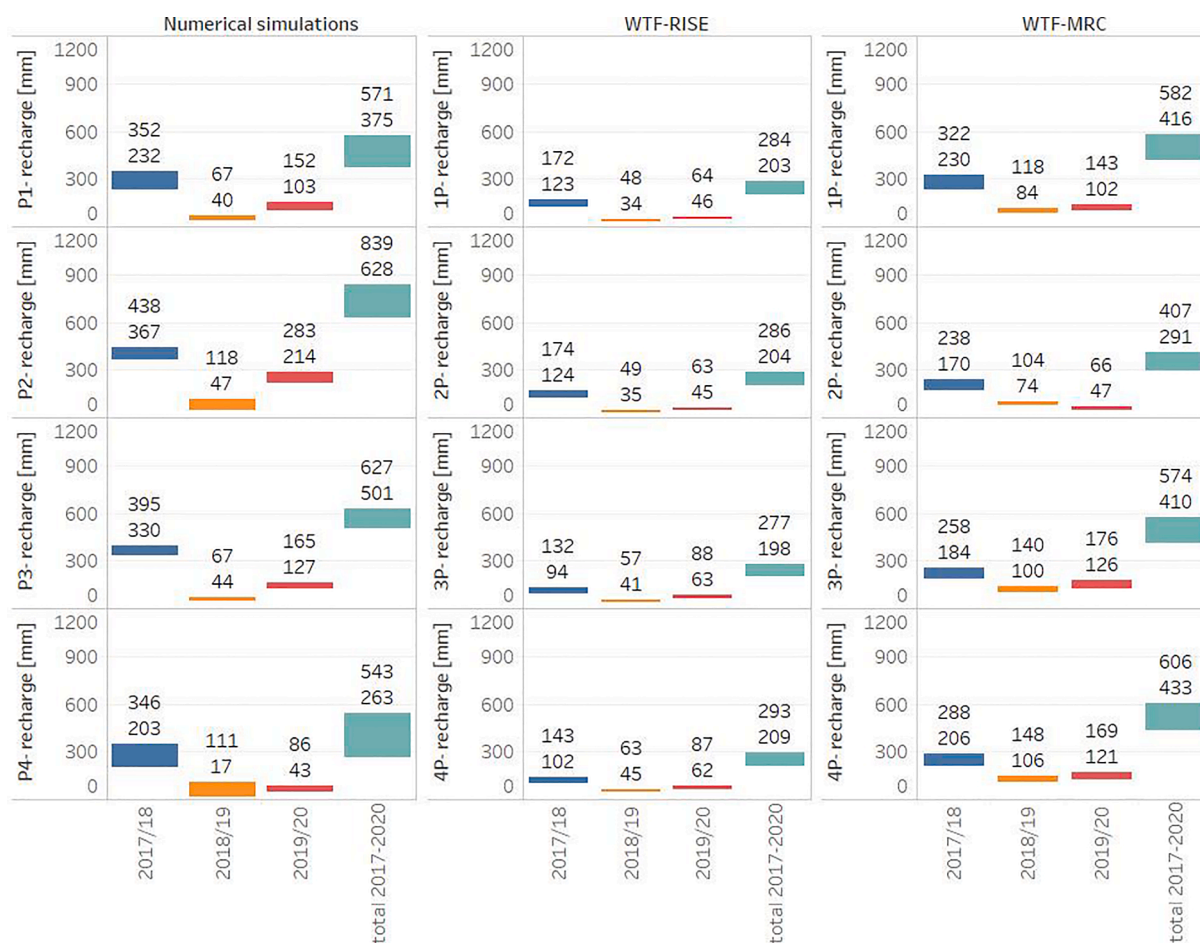
Fig. 6. Recharge estimates obtained using different methods. For numerical simulations, the range of results corresponds to the assumed range of LAI values in each profile. For WTF, the range of results corresponds to the assumed range of specific yield values in the aquifer.

discharge to lakes is partly compensated for by recharge from infiltration.

Recharge rates calculated for each profile using the RISE and MRC methods and different estimates of S_y are shown in Fig. 6, together with the results of numerical simulations discussed earlier. Several conclusions can be drawn from this comparison. The estimates obtained using the MRC method are more than twice as large as those obtained using the RISE method, emphasizing the importance of including a recession curve in the analysis. In most cases, the results of numerical simulations are closer to MRC than to RISE, except for the second (driest) observation year, where the opposite is true. In this period, recharge is low and thus sensitive to inaccuracies in the approximation of the recession curve.

Considering the whole 3-year period, we can notice a good agreement between the MRC method and the HYDRUS-1D simulations for the forest profiles (P1 and P4) with the lower LAI (2.10) and for the P3 profile (grass with an LAI of 2.90). The numerical results fall between the MRC estimates for low and high S_y (410 mm to 606 mm). In contrast, the largest discrepancy between numerical modeling and the WTF analysis occurs for P2. In this case, even for the highest value of specific yield, the MRC estimate is significantly smaller than the lowest value obtained using the numerical model. These observations further support the conclusions from Section 4.4 that the simulations for P1 with a low LAI and P3 with a high LAI yield recharge patterns, which are the most consistent with the observed groundwater level fluctuations, while the largest incompatibility is observed for P2. The disagreement for P2 is probably caused by two overlapping effects: increased local recharge due to the high permeability of the sandy loam layer and a possible

malfunction of the water level sensor.

Further cross-validation of the WTF method and numerical modeling can be done following Jie et al. (2011). The sum of the water table increments calculated using the MRC approach for P1 is 2080 mm in the 3-year period, while the corresponding recharge obtained using the HYDRUS-1D simulation with an LAI of 2.10 is 571 mm. This provides an estimate of S_y (=571 mm/2080 mm) of 0.274, very close to the value calculated using the water balance in the numerical solution with lateral outflow (0.278) and within the range given by Healy (2010). Similarly, for P3, the sum of increments is 2050 mm, and the recharge estimate using Hydrus (LAI = 2.90) is 501 mm for $S_y = 0.244$. Again, this value is very close to the estimate derived directly from the numerical simulation with lateral outflow (0.233). This analysis increases the confidence in the recharge estimates provided by numerical simulations.

4.7. Time variability of recharge and a recharge/precipitation ratio

The presented results show that groundwater recharge is a time-variable process and, at least on a short time scale, cannot be considered as steady-state flow. The time distribution of groundwater recharge is strongly determined by the intensity and distribution of precipitation. Abundant rainfalls in 2017 resulted in high inflow to the water table in autumn/winter 2017/2018. On the contrary, the drought in 2018 caused a drop in the water table and low percolation from the vadose zone to the aquifer in winter/spring 2019. In the last year of the observations (2019/20), both precipitation and recharge were between the two earlier extreme years. In Table 4, we report annual and total recharge estimates based on three numerical simulations that were
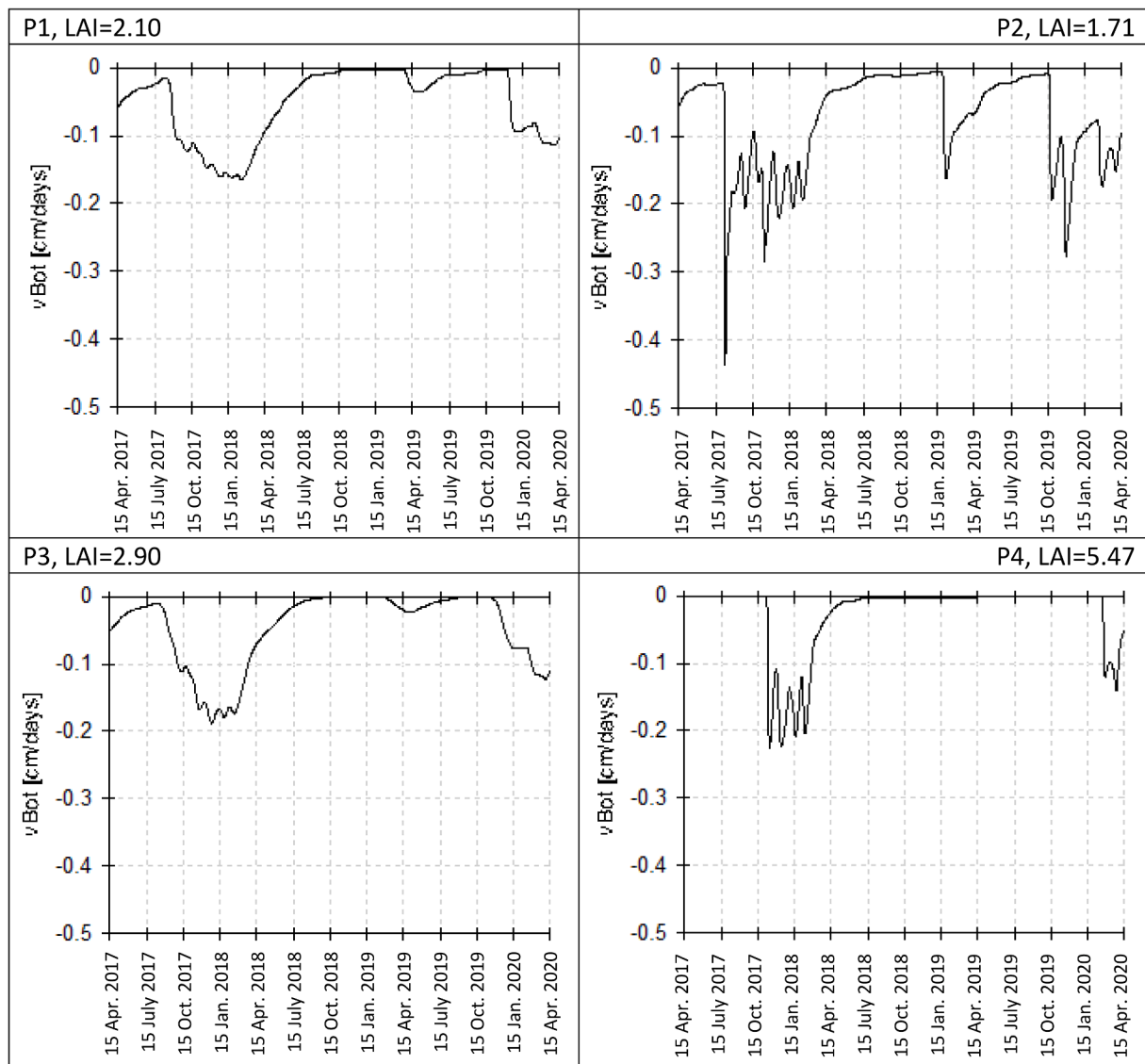
Fig. 7. The recharge flux (vBot in Hydrus 1D) at the groundwater table obtained using numerical simulations with a constant water table position.

found to be the most representative for the study area (P1-LAI 2.10, P3-LAI 2.90, P4-LAI 2.10). The ratio of annual recharge between the first (wet) and second (dry) year of observations ranged from 3.1 (P4-LAI 2.10) to 7.5 (P3-LAI 2.90). The ratios obtained using WTF were smaller, but still significant: 2.3 to 3.6 in the RISE method and 1.8 to 2.7 in the MRC method.

The time of the water table response to a single rain event depends on the thickness of the unsaturated zone, soil type, and vegetation. Since the magnitude of the water table rise is determined by the water content in the unsaturated zone, the amount of precipitation during the preceding weeks plays a significant role (Dripps, 2012). That is probably the reason why groundwater recharge following the storm at the end of June 2017, which occurred after wet months, is so apparent. On July 17, 2018, even more abundant rainfalls (47 mm/day) took place. However, this event did not result in any response of the water table, probably because of the dry preceding spring and summer.

Some studies provide guidelines to estimate annual or multi-year recharge in Central Europe as a specific fraction of precipitation, depending on the soil type, land cover, and other factors (Dyck and Chardebellas, 1963, cited after Hölting and Coldewey, 2019; Duda et al., 2011). Hölting and Coldewey (2019) provide an empirical formula for the annual recharge-precipitation relationship based on an earlier study

of Dyck and Chardabellas (1963), who summarized data from a large number of lysimeters:

$$R = 1.1 \cdot P - \Delta P \tag{10}$$

where P is annual precipitation and ΔP depends on soil and land cover. For sandy soils with vegetation, $\Delta P = 433$ mm, and the corresponding results are shown in Table 4. Eq. (10) provides recharge estimates significantly larger than the numerical simulations and WTF applied to our site, except for the driest year, for which the agreement is reasonable. It should be noted that R in Eq. (10) corresponds to the drainage flux measured in lysimeters, which can be significantly larger than recharge, if there is a possibility of upward capillary flow or water uptake by plant roots from depths below the bottom of the lysimeter. Moreover, Eq. (10) does not account for the presence of low permeability layers, which was the case on our site.

Another simple formula relating recharge to precipitation over annual or longer time scales is:

$$R = \omega \cdot P \tag{11}$$

where $\omega = R/P$ is the recharge–precipitation ratio, which depends on various factors. Pazdro & Kozerski (1990) suggested $\omega = 0.25$ to 0.3 for
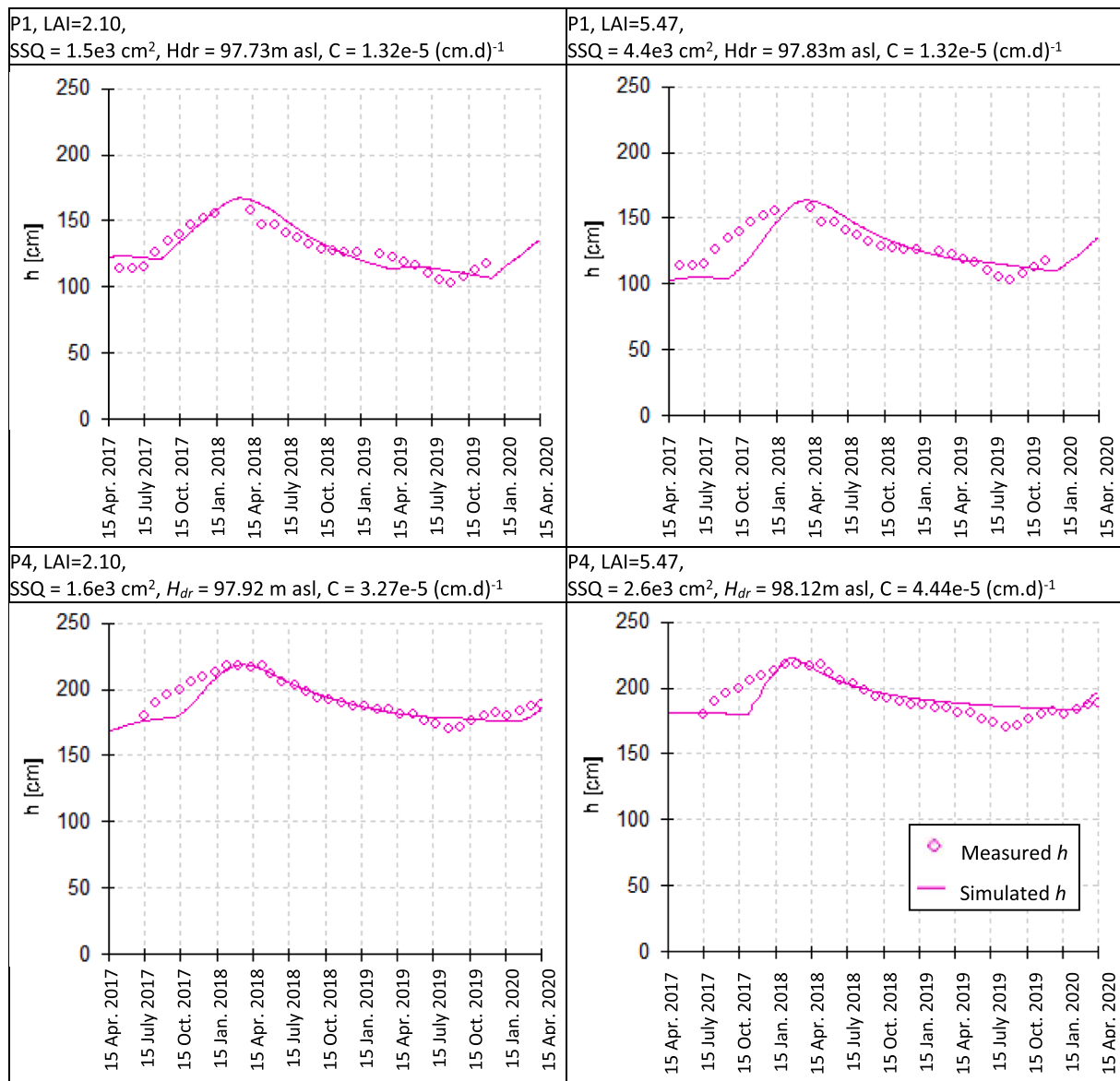
P1, LAI=2.10,
SSQ = 1.5e3 cm^2, Hdr = 97.73m asl, C = 1.32e-5 (cm.d)$^{-1}$

P1, LAI=5.47,
SSQ = 4.4e3 cm^2, Hdr = 97.83m asl, C = 1.32e-5 (cm.d)$^{-1}$

P4, LAI=2.10,
SSQ = 1.6e3 cm^2, H_{dr} = 97.92 m asl, C = 3.27e-5 (cm.d)$^{-1}$

P4, LAI=5.47,
SSQ = 2.6e3 cm^2, H_{dr} = 98.12m asl, C = 4.44e-5 (cm.d)$^{-1}$

Fig. 8. Measured and simulated positions of the groundwater table (*h*, measured with respect to the profile bottom), representing the best fit for each profile obtained using simulations with lateral outflow – forest profiles P1 and P4.

glacial and fluvioglacial sands, such as those occurring on the Brda outwash plain. The *R/P* ratio for the whole 3-year observation period obtained using numerical simulations (0.24–0.28) and from WTF-MRC (0.20–0.30) is close to this estimate. In the more recent study by Duda et al. (2011), ω was assumed to be a product of four partial coefficients: $\omega = \alpha\beta\,\gamma\delta$, representing the soil type (*α*), land cover (β), ground slope (*γ*), and depth to groundwater table (*δ*). The suggested *α* value for sandy deposits is 0.14 to 0.22, while β is 1 for grassland and 0.9 for forests. In our case, the factors *γ* and *δ* were equal to 1, because the terrain is relatively flat and the depth to the groundwater table is more than 2 m. This gives a range of ω values from 0.14 to 0.22 for grassland and 0.13 to 0.20 for the forest. The resulting recharge estimates are quite close to the numerical simulations and WTF-MRC in the second (dry) and third (average) years, while they are significantly lower in the first (wet) year and, consequently, also in terms of the total 3-year recharge. The co-efficients suggested by Duda et al. (2011) were inferred from the base-flow analysis for several Polish rivers. Regional (watershed) scale recharge estimated from baseflow tends to be smaller than local-scale estimations in areas with the groundwater table below the root zone

because a part of recharged groundwater is lost to evapotranspiration in river valleys and wetlands before discharging to the river. However, recharge estimates for the region of our experimental site (an upper Brda river watershed, Hobot et al., 2012) obtained from baseflow measure-ments are about 155 to 193 mm/yr (26% to 33% of the average pre-cipitation in Chojnice), which is in good agreement with the results of our numerical simulations (an average of the 3-year period is 167 to 191 mm/yr).

Since the plant water demand does not change from one year to the other as much as precipitation, the fraction of total precipitation reaching groundwater is smaller in dry years than in wet years (Kowalski, 2007). This is consistent with the results of numerical sim-ulations, which indicate a much larger *R/P* ratio for the wettest year (0.36–0.38) than the driest year (0.10–0.24). According to the WTF-MRC method, the variability of the *R/P* ratio is smaller, and the lowest *R/P* ratio is in the third year, representing average conditions between wet and dry years. Eq. (10) predicts a very strong dependence of the *R/P* ratio on precipitation, which is not reflected in our results. In contrast, Eq. (11) provides a constant ratio $\omega = R/P$, i.e. the recharge is a
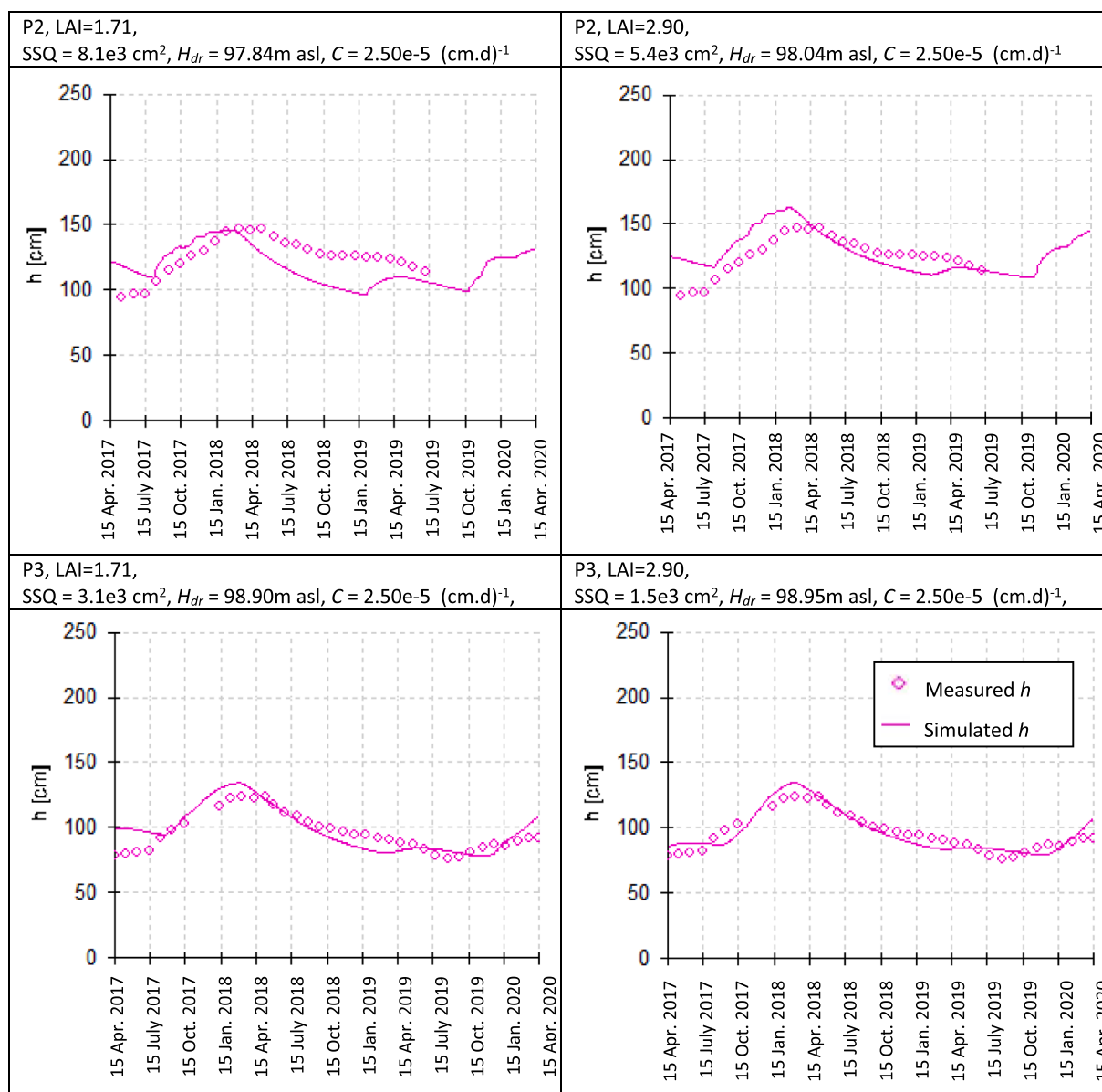
P2, LAI=1.71,
SSQ = 8.1e3 cm², H_{dr} = 97.84m asl, C = 2.50e-5 (cm.d)⁻¹

P2, LAI=2.90,
SSQ = 5.4e3 cm², H_{dr} = 98.04m asl, C = 2.50e-5 (cm.d)⁻¹

P3, LAI=1.71,
SSQ = 3.1e3 cm², H_{dr} = 98.90m asl, C = 2.50e-5 (cm.d)⁻¹,

P3, LAI=2.90,
SSQ = 1.5e3 cm², H_{dr} = 98.95m asl, C = 2.50e-5 (cm.d)⁻¹,

Fig. 9. Measured and simulated positions of the groundwater table (*h*, measured with respect to the profile bottom), representing the best fit for each profile obtained using simulations with lateral outflow – grassland profiles P2 and P3.

fixed fraction of annual precipitation regardless of the actual amount of precipitation. Neither of these equations appeared adequate in our case. However, Eq. (11) seems to work reasonably well in dry or average years.

The increasing occurrence of extremely wet and dry periods along with temperature rise leading to higher evapotranspiration and shorter snow season are the main symptoms of climate change in Central Europe (Goudie, 2006; IPCC, 2021), which in turn affect groundwater recharge (eg., Haidu and Nistor, 2019; Jaworska-Szulc, 2015; Neukum and Azzam, 2012;). Our modeling approach seems to be a promising tool to evaluate recharge under different historical or future climate change scenarios (Gumuła-Kawęcka et al. 2021). In particular, it is possible to represent groundwater table fluctuations using a 1D variably-saturated flow model, if the parameters describing lateral outflow are known. They can be obtained from limited time series of water table measurements, and the model can be further enhanced by including time-variable water level in the surface water body (lake or stream).

4.8. Influence of plant cover

It could be expected that recharge in a forest is smaller than in a grassland area due to higher interception by the tree canopy and the ability of tree roots to extract water from larger depths. However, there does not appear to be a universal relationship between recharge in forests and grasslands, since it may depend on particular plant species. According to Dripps & Bradbury (2010), recharge under the coniferous forest was only slightly smaller than under grass cover. Grinevskii & Novoselova (2011) found that recharge under the forest was actually larger than under cropland.

In our simulations, recharge depended strongly on LAI. On average, recharge estimates for the grassland profiles were larger than for the forest profiles (Fig. 6) because the assumed range of LAI values was higher for the forest than for grassland, despite a partial overlap. However, looking only at the three scenarios, which showed the best agreement with the observed water table fluctuations, we can see that recharge in the grassland profile P3 (LAI 2.9) was actually lower than in P1 or P4 (with an LAI of 2.1). This is a consequence of our choice of LAI
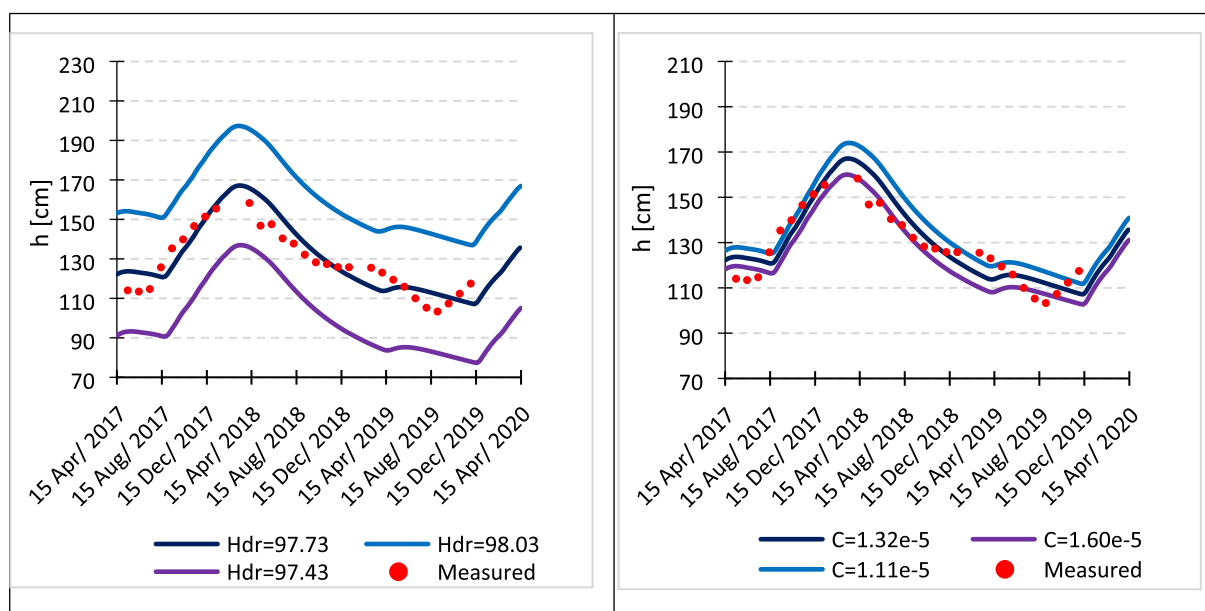
Fig. 10. Sensitivity of the water table position in profile P1 (h, measured with respect to the profile bottom) to the parameters of lateral outflow boundary condition: H_{dr} [m asl] (left) and C [(cm.d)$^{-1}$] (right).
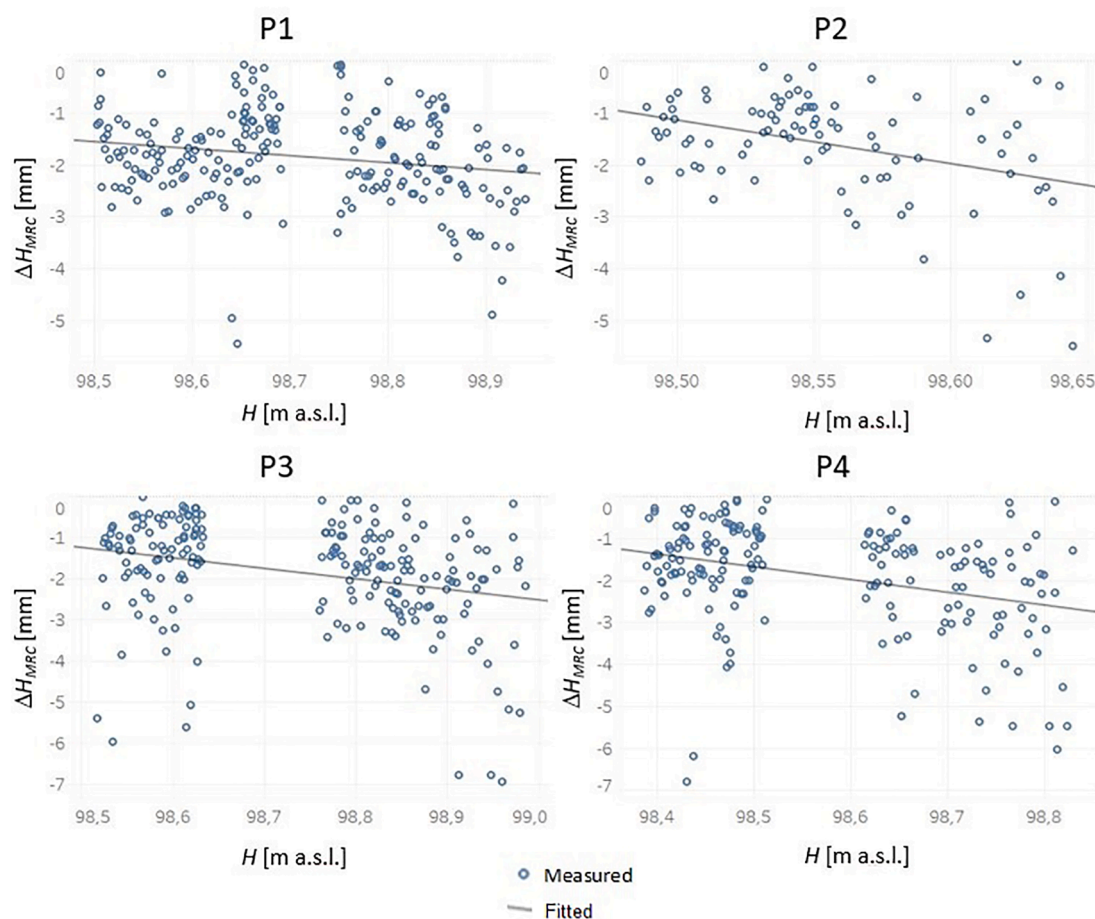

Fig. 11. Master recession curves (MRC) representing the relationship between the groundwater table elevation (H [m a.s.l.]) and daily decrements of the water level (ΔH_{MRC} [mm]).
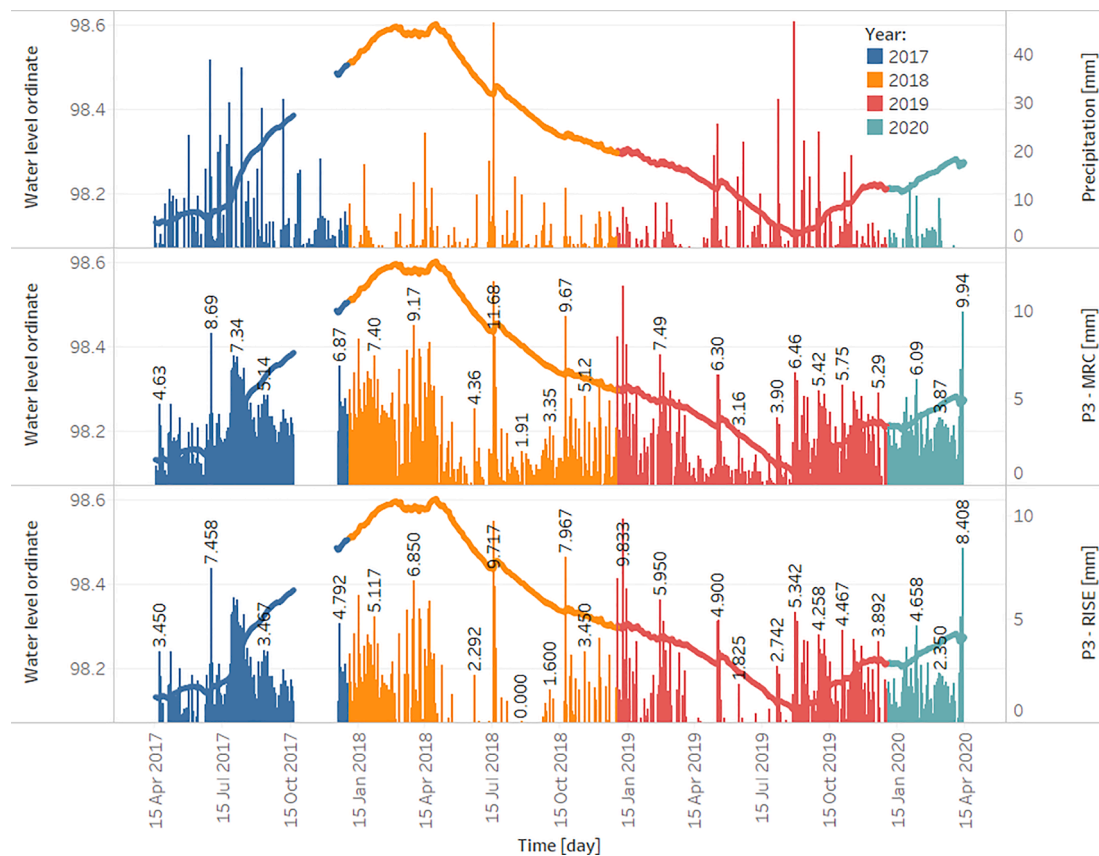
Fig. 12. Increments of groundwater table caused by recharge in profile P3, according to the RISE and MRC methods.

Table 4
Recharge (*R*) and recharge/precipitation ratios ($\omega = R/P$) obtained from numerical simulations WTF (MRC) and simple estimation methods.

	Simulations		MRC		Eq. (10)		Eq. (11)	
	R [mm]	*R/P* [-]	*R* [mm]	*R/P* [-]	*R* [mm]	*R/P* [-]	*R* [mm]	*R/P* [-]
2017/18	330–352	0.36–0.38	184–322	0.20–0.35	579	0.63	120–202	0.13–0.22
2018/19	44–111	0.10–0.24	84–148	0.18–0.32	76	0.16	60–102	0.13–0.22
2019/20	86–152	0.13–0.23	102–176	0.15–0.26	304	0.46	87–147	0.13–0.22
total	501–573	0.24–0.28	410–606	0.20–0.30	959	0.47	267–452	0.13–0.22

values for the simulations, with the upper estimate for grass higher than the lower estimate for pine forest, as explained in Section 3.3. Our results emphasize the need for accurate estimations of LAI. However, identification of actual LAI values in the study area and their possible evolution in time was outside the scope of the present work.

In contrast, WTF did not show significant differences in recharge between grassland and forest profiles. The results of the WTF method are affected by the land cover in a larger area, not only in the close vicinity of the monitoring well. Forests are intermixed with open grasslands, crop fields, and small built-up regions in our study area. Consequently, water table fluctuations in both monitoring wells showed a similar pattern, representing average recharge.

5. Conclusion

This study highlights the need to use multiple methods and observation periods to increase confidence in recharge estimations, especially given the increasing occurrence of extremely wet and dry periods in temperate climate zone. In our approach, numerical simulations of vertical flow in the vadose zone were combined with the analysis of water table fluctuations. We showed how these two methods could inform and cross-validate each other. Using a modified boundary

condition in numerical simulations, one can check if the vadose zone model is consistent with the observed groundwater table fluctuations. An additional benefit is the calculation of specific yield from the simulation results. The specific yield can be later used in the WTF-MRC analysis to see if the recharge estimates are consistent with those obtained from simulations.

One can note a conceptual similarity between the numerical simulations with the modified bottom boundary condition and the master recession curve (MRC) approach. In both cases, the aim is to include lateral groundwater flow in the analysis of point-scale observations. In this way, we can obtain a more accurate description of the vadose zone – groundwater interactions without the need to solve more complex 2D or 3D models.

The incorporation of groundwater level observations in vadose zone models significantly reduces the uncertainty in recharge estimations. Our results showed that soil water measurements alone are insufficient to constrain the models, especially if there is no detailed data on evapotranspiration.

In view of the significant year-to-year variability of precipitation and recharge, numerical simulations and WTF should preferably be applied on longer time scales to achieve meaningful recharge estimations. In numerical simulations, it is important to use a warm-up period with

realistic weather data to accurately reproduce the initial state of soil water.

Further research is warranted on the combined use of 1D numerical models and WTF. In particular, there is a need to investigate other analytical formulas describing the lateral outflow boundary condition and to develop tools for calibrating their parameters jointly with the calibration of soil hydraulic parameters and/or ET-related parameters. We believe that the approach presented here can be used to improve recharge estimates in unconfined aquifers over a wide range of geological and hydrological settings.

CRediT authorship contribution statement

Anna Gumuła-Kawęcka: Conceptualization, Formal analysis, Investigation, Methodology, Writing – original draft. **Beata Jaworska-Szulc:** Conceptualization, Formal analysis, Investigation, Methodology. **Adam Szymkiewicz:** Conceptualization, Formal analysis, Methodology, Writing – original draft. **Wioletta Gorczewska-Langner:** Formal analysis, Investigation. **Małgorzata Pruszkowska-Caceres:** Investigation. **Rafael Angulo-Jaramillo:** Methodology, Investigation, Writing – review & editing. **Jirka Šimůnek:** Methodology, Software, Writing – review & editing.

Declaration of Competing Interest

The authors declare that they have no known competing financial interests or personal relationships that could have appeared to influence the work reported in this paper.

Acknowledgments

References

Åberg, S.C., Korkka-Niemi, K., Rautio, A., Salonen, V.P., Åberg, A., 2019. Groundwater recharge/discharge patterns and groundwater–surface water interactions in a sedimentary aquifer along the River Kitinen in Sodankylä, northern Finland. Boreal Environ. Res. 24, 155–187.

Ala-aho, P., Rossi, P.M., Kløve, B., 2014. Estimation of temporal and spatial variations in groundwater recharge in unconfined sand aquifers using Scots pine inventories. Hydrol. Earth Syst. Sci. Discuss. 11, 7773–7826.

Allen, R.G., Pereira, L.S., Raes, D., Smith, M., 1998. Crop evapotranspiration-Guidelines for computing crop water requirements-FAO Irrigation and drainage paper 56. Fao, Rome, 300(9), D05109.

Batalha, M.S., Barbosa, M.C., Faybishenko, B., van Genuchten, M.T., 2018. Effect of temporal averaging of 381 meteorological data on predictions of groundwater recharge. J. Hydrol. Hydromech. 66, 143–152.

Batelaan, O., De Smedt, F., 2001. WetSpass: a flexible, GIS based, distributed recharge methodology for regional groundwater modelling. IAHS PUBLICATION 11–18.

Beegum, S., Šimůnek, J., Szymkiewicz, A., Sudheer, K., Nambi, I., 2018. Updating the coupling algorithm between HYDRUS and MODFLOW in the HYDRUS package for MODFLOW. Vadose Zone J. 17 (1), 1–8.

Bouwer, H., 1989. Estimating and enhancing groundwater recharge. In: Sharma, M.L. (Ed.), Grounwater recharge. A.A, Balkema, Rotterdam, pp. 1–10.

Braden, H., 1985. Ein Energiehaushalts- und Verdunstungsmodell for Wasser und Stoffhaushaltsuntersuchungen landwirtschaftlich genutzer Einzugsgebiete. Mittelungen Deutsche Bodenkundliche Geselschaft, 42, 294-299.

Brunner, P., Doherty, J., Simmons, C.T., 2012. Uncertainty assessment and implications for data acquisition in support of integrated hydrologic models. Water Resour. Res. 48 (7), W07513.

Callahan, T.J., Vulava, V.M., Passarello, M.C., Garrett, C.G., 2012. Estimating groundwater recharge in lowland watersheds. Hydrol. Process. 26 (19), 2845–2855.

Carsel, R.F., Parrish, R.S., 1988. Developing joint probability distributions of soil water retention characteristics. Water Resour. Res. 24 (5), 755–769.

Cherkauer, D.S., Ansari, S.A., 2005. Estimating ground water recharge from topography, hydrogeology, and land cover. Ground Water 43 (1), 102–112.

Delin, G.N., Healy, R.W., Lorenz, D.L., Nimmo, J.R., 2007. Comparison of local-to regional-scale estimates of ground-water recharge in Minnesota, USA. J. Hydrol. 334 (1-2), 231–249.

De Silva, M.S., Nachabe, M.H., Šimůnek, J., Carnahan, R., 2008. Simulating root water uptake from a heterogeneous vegetative cover. J. Irrig. Drain. Engin.-ASCE 134 (2), 167–174.

de Vries, J.J., Simmers, I., 2002. Groundwater recharge: an overview of processes and challenges. Hydrogeol. J. 10 (1), 5–17.

Dripps, W.R., 2012. An integrated field assessment of groundwater recharge. Open Hydrol. J. 6 (1), 15–22.

Dripps, W.R., Bradbury, K.R., 2010. The spatial and temporal variability of groundwater recharge in a forested basin in northern Wisconsin. Hydrol. Process. 24, 383–392.

Duda, R., Witczak, S., Żurek, A., 2011. Mapa wrażliwości wód podziemnych na zanieczyszczenie w skali 1:500 000 [Groundwater vulnerability map of Poland 1:500 000]. Akademia Górniczo-Hutnicza im. S, Staszica w Krakowie, Kraków.

Dyck, P.P., Chardabellas, P., 1963. Wege zur Ermittlung der nutzbaren Grundwasserreserven. Ber. Geol. Ges DDR 8, 245–262.

Feddes, R.A., Kowalik, P.J., Zaradny, H., 1978. Simulation of Field Water Use and Crop Yield. John Wiley & Sons, New York, NY.

Goudie, A.S., 2006. Global warming and fluvial geomorphology. Geomorphology 79 (3-4), 384–394.

Graf, R., Przybyłek, J., 2014. Estimation of shallow groundwater recharge using a GIS-based distributed water balance model. Quaestiones Geographicae 33 (3), 7–37.

Grinevskii, S.O., Novoselova, M.V., 2011. Regularities in the formation of groundwater infiltration recharge. Water Resour. 38 (2), 175–186.

Gumuła-Kawęcka, A., Jaworska-Szulc, B., Szymkiewicz, A., Gorczewska-Langner, W., 2021. Impact of climate change on groundwater recharge in shallow sandy aquifer (Brda outwash plain, Pomeranian Region, Northern Poland). Subbmited.

Gumuła-Kawęcka, A., Szymkiewicz, A., Jaworska-Szulc, B., Pruszkowska-Caceres, M., Gorczewska-Langner, W., Kaźmierczak, B., Kutyłowska, M., Piekarska, K., Jadwiszczak, P., 2018. Preliminary estimation of groundwater recharge on Brda river outwash plain. E3S Web Conf. 44, 00050. https://doi.org/10.1051/e3sconf/20184400050.

Haidu, I., Nistor, M.M., 2019. Long-term effect of climate change on groundwater recharge in the Grand Est region of France. Meteorol. Appl. 27 (1), 1–17.

He, J., Hantush, M.M., Kalin, L., Rezaeianzadeh, M., Isik, S., 2021. A two-layer numerical model of soil moisture dynamics: model development. J. Hydrol. 602, 126797. https://doi.org/10.1016/j.jhydrol.2021.126797.

Healy, R. W., 2010. Estimating groundwater recharge. Cambridge University Press, Cambridge.

Heppner, C.S., Nimmo, J.R. 2005. A computer program for predicting recharge with a master recession curve. U.S. Geological Survey Scientific Investigations Report 2005-5172.

Heppner, C.S., Nimmo, J.R., Folmar, G.J., Gburek, W.J., Risser, D.W., 2007. Multiple-methods investigation of recharge at a humid-region fractured Rock Site, Pennsylvania, USA. Hydrogeol. J. 15 (5), 915–927.

Hobot, A., Banaszak, K., Stolarska, M., Sowińska, K., Serafin, R., Stachura, A., 2012. Warunki korzystania z wód zlewni rzeki Brdy, Etap 1 – Dynamiczny bilans ilościowy zasobów wodnych [Conditions of water usage in Brda river watershed, Stage 1 – Dynamic water budget], report for Regional Water Management Office in Gdańsk. Pectore-Eco company, Gliwice.

Hölting, B., Coldewey, W.G., 2019. Hydrogeology. Springer.

Huet, M., Chesnaux, R., Boucher, M.-A., Poirier, C., 2016. Comparing various approaches for assessing groundwater recharge at a regional scale in the Canadian Shield. Hydrolog. Sci. J. 61 (12), 2267–2283.

Ines, A.V.M., Mohanty, B.P., 2008. Near-surface soil moisture assimilation for quantifying effective soil hydraulic properties using genetic algorithm: 1. Conceptual modeling. Water Resour. Res. 44, W06422.

IPCC, 2021. Summary for Policymakers. In: Climate Change 2021: The Physical Science Basis. Contribution of Working Group I to the Sixth Assessment Report of the Intergovernmental Panel on Climate Change, Cambridge University Press. In Press.

Jackson, R.B., Canadell, J., Ehleringer, J.R., Mooney, H.A., Sala, O.E., Schulze, E.D., 1996. A global analysis of root distributions for terrestrial biomes. Oecologia 108 (3), 389–411.

Jagodziński, A.M., Kałucka, I., 2008. Age-related changes in leaf area index of young Scots pine stands. Dendrobiology 59, 57–65.

Jaworska-Szulc, B., 2015. Impact of climate change on groundwater resources in a young glacial multi-aquifer system. Pol. J. Environ. Stud. 24 (6), 2447–2457.

Jaworska-Szulc, B., Pruszkowska-Caceres, M., Szymkiewicz, A., Gumuła-Kawęcka, A., Gorczewska-Langner, W., 2017. Wahania zwierciadła płytkich wód podziemnych na obszarze sandrowym w rejonie Chojnic [Groundwater table fluctuations in the shallow aquifer of the Brda River outwash plain]. Przegląd Geologiczny 65 (11), 247–255.

Jie, Z., van Heyden, J., Bendel, D., Barthel, R., 2011. Combination of soil-water balance models and water-table fluctuation methods for evaluation and improvement of groundwater recharge calculations. Hydrogeol. J. 19 (8), 1487–1502.

Johnson, A.I., 1967. Specific yield: compilation of specific yields for various materials. US Geological Survey Water-Supply Paper 1662-D.

Kowalski, J., 2007. Hydrogeologia z podstawami geologii [Hydrogeology and elements of geology], third ed. Wydawnictwo Uniwersytetu Przyrodniczego we Wrocławiu, Wrocław.

Krogulec, E., 2010. Evaluation of infiltration rates within the Vistula Rivervalley, central Poland. Acta Geol. Polonica 60 (4), 617–628.

Kurylyk, B.L., MacQuarrie, K.T.B., 2013. The uncertainty associated with estimating future groundwater recharge: A summary of recent research and an example from a small unconfined aquifer in a northern humid-continental climate. J. Hydrol. 492, 244–253.

Lerner, D.N., Isaar, A.S., Simmers, I., 1990. Groundwater Recharge: A Guide to Understanding and Estimating Natural Recharge, International Contributions to Hydrogeology. Verlag Heinz Heise, Hanover.

Leterme, B., Mallants, D., 2011. Climate and land use change impacts on groundwater recharge. Proceedings ModelCARE2011. Models - Repositories of Knowledge. IAHS Publ., Leipzig, Germany, 18-22 September 2011.

Leterme, B., Mallants, D., Jacques, D., 2012. Sensitivity of groundwater recharge using climatic analogues and HYDRUS-1D. Hydrol. Earth Syst. Sci. 16 (8), 2485–2497.

Liu, Y., Yamanaka, T., Zhou, X., Tian, F., Ma, W., 2014. Combined use of tracer approach and numerical simulation to estimate groundwater recharge in an alluvial aquifer system: a case study of Nasunogahara area, central Japan. J. Hydrol. 519, 833–847.

Muter, K., 2002. Mapa Hydrogeologiczna Polski w skali 1:50 000, ark. Cekcyn (204) [Hydrogeological Map of Poland 1:50 000, sheet Cekcyn (204)]. PIG, Warszawa.

Nastev, M., Rivera, A., Lefebvre, R., Martel, R., Savard, M., 2005. Numerical simulation of groundwater flow in regional rock aquifers, southwestern Quebec, Canada. Hydrogeol. J. 13 (5-6), 835–848.

Neukum, C., Azzam, R., 2012. Impact of climate change on groundwater recharge in a small catchment in the Black Forest, Germany. Hydrogeol. J. 20 (3), 547–560.

Nimmo, J.R., Horowitz, Ch., Mitchell, L., 2015. Discrete-storm water-table fluctuation method to estimate episodic recharge. Groundwater 53(2), 282–292.

Niswonger, R., Prudic, D., Regan, R., 2006. Documentation of the Unsaturated-Zone Flow (UZF1) Package for modeling unsaturated flow between the land surface and the water table with MODFLOW-2005: U.S. Geological Techniques and Methods Book 6, Chapter A19.

Oficjalska, H., Gregosiewicz, R., 2000. Mapa Hydrogeologiczna Polski w skali 1:50 000, ark. Tuchola (203) [Hydrogeological Map of Poland 1:50 000, sheet Tuchola (203)]. PIG, Warszawa.

Pazdro, Z., Kozerski, B., 1990. Hydrogeologia ogólna [Hydrogeology]. Wydawnictwa Geologiczne, Warszawa.

Pozdniakov, S., Vasilevskiy, P., Grinevskiy, S., 2015. Estimation of groundwater recharge by flow in vadose zone simulation at the watershed with different landscapes and soil profiles. Engin. Geol. Hydrogeol. Bulgarian Acad. Sci. 29, 47–58.

Puchalski, T., Prusinkiewicz, Z., 1990. Ekologiczne podstawy siedliskoznawstwa leśnego [Ecological foundations of forest habitats]. PWRiL, Warszawa.

Rutkowski, P., Samborska, K., Wajsowicz, T., Konatowska, M., Budka, A., Maciejewska-Rutkowska, I., Rybarczyk, A., 2017. Rozmieszczenie korzeni trzech gatunków drzew w glebach Słowińskiego Parku Narodowego [Distribution of roots of three tree species in soils of Słowiński National Park]. Acta Scientiarum Polonorum. Silvarum Colendarum Ratio et Industria Lignaria 16 (4).

Sainju, U.M., Good, R.E., 1993. Vertical root distribution in relation to soil properties in New Jersey Pinelands forests. Plant Soil 150 (1), 87–97.

Scanlon, B.R., Healy, R.W., Cook, P.G., 2002a. Choosing appropriate techniques for quatifying groundwater recharge. Hydrogeol. J. 10, 18–39.

Scanlon, B.R., Christman, M., Reedy, R.C., Porro, I., J., Flerchinger, G.N., 2002b. Intercode comparisons for simulating water balance of surficial sediments in semiarid regions. Water Resour. Res. 38 (12), 1323.

Schroeder, P.R., Dozier, T.S., Zappi, P.A., McEnroe, B.M., Sjostrom, J.W., Peyton, R.L., 1994. Hydrologic Evaluation of Landfill Performance (HELP) model. Engineering Documentation for Version 3.0. U.S. Environmental Protection Agency, Risk Reduction Engineering Laboratory, Cincinnati, OH, USA.

Scurlock, J. M. O., Asner, G. P., & Gower, S. T. (2001). Worldwide historical estimates of leaf area index, 1932–2000. ORNL/TM-2001/268, 34.

Şen, Z., 2015. Applied Drought Modelling, Prediction, and Mitigation. The, first ed. Elsevier, Amsterdam.

Simmers, I., 1997. Recharge of Phreatic Aquifers in (Semi-) Arid Areas. A. A Balkema, Rotterdam.

Šimůnek, J., Šejna, M., Saito, H., Sakai, M., van Genuchten, M.T., 2013. The HYDRUS-1D Software Package for Simulating theOne-Dimensional Movement of Water, Heat,

and Multiple Solutes in Variably-Saturated Media. Version 4.17. Department of Environmental Sciences. University of California Riverside, Riverside, CA, USA.

Šimůnek, J., van Genuchten, M., Šejna, M., 2008. Development and applications of the HYDRUS and STANMOD software packages and related codes. Vadose Zone J. 7 (2), 587–600.

Šimůnek, J., van Genuchten, M.T., Šejna, M., 2016. Recent developments and applications of the HYDRUS computer software packages. Vadose Zone J. 15 (7).

Smerdon, B.D., Mendoza, C.A., Devito, K.J., 2008. Influence of subhumid climate and water table depth on groundwater recharge in shallow outwash aquifers. Water Resour. Res. 44, W08427.

Sophocleous, M.A., 1991. Combing the soil-water balance and water-level fluctuation methods to estimate natural groundwater recharge: practical aspects. J. Hydrol. 124, 229–241.

Sousa, M.R., Jones, J.P., Frind, E.O., Rudolph, D.L., 2013. A simple method to assess unsaturated zone time lag in the travel time from ground surface to receptor. J. Contam. Hydrol. 144, 138–151.

Szilagyi, J., Zlotnik, V., Gates, J.B., Jozsa, J., 2011. Mapping mean annual groundwater recharge in the Nebraska Sand Hills. USA. Hydrogeol. J. 19, 1503–1513.

Szymkiewicz, A., Gumuła-Kawęcka, A., Šimůnek, J., Leterme, B., Beegum, S., Jaworska-Szulc, B., Pruszkowska-Caceres, M., Gorczewska-Langner, W., Angulo-Jaramillo, R., Jacques, D., 2018a. Simulation of the freshwater lens recharge using the HYDRUS and SWI2 packages for MODFLOW. J. Hydrol. Hydromech. 66, 246–256.

Szymkiewicz, A., Gumuła-Kawęcka, A., Potrykus, D., Jaworska-Szulc, B., Pruszkowska-Caceres, M., Gorczewska-Langner, W., 2018b. Estimation of conservative contaminant travel time through vadose zone based on transient and steady flow approaches. Water 10 (10), 1417.

Szymkiewicz, A., Savard, J., Jaworska-Szulc, B., 2019. Numerical analysis of recharge rates and contaminant travel time in layered unsaturated soils. Water 11 (3), 545.

Szymkiewicz, A., Potrykus, D., Jaworska-Szulc, B., Gumuła-Kawęcka, A., Pruszkowska-Caceres, M., Dzierzbicka-Głowacka, L., 2020. Evaluation of the influence of farming practices and land use on groundwater resources in a coastal multi-aquifer system in Puck region (northern Poland). Water 12 (4), 1042.

Twarakavi, N., Šimůnek, J., Seo, S., 2008. Evaluating Interactions between groundwater and vadose zone using the HYDRUSbased flow package for MODFLOW. Vadose Zone J. 7, 757–768.

van Dam, J.C., Huygen, J., Wesseling, J.G., Feddes, R.A., Kabat, P., van Walsum, P.E.V., Groenendijk, P., van Diepen, C.A., 1997. Theory of SWAP version 2.0, Report 71, Dept. of Water Resour. Wageningen Agricultural University, Wageningen, the Netherlands.

van Genuchten, M.T., 1980. A closed form equation for predicting the hydraulic conductivity of unsaturated soils. Soil Sci. Soc. Am. J. 44, 892–898.

Von Hoyningen-Hüne, J., 1983. Die Interception des Niederschlags in landwirtschaftlichen Beständen. Schriftenreihe des DVWK 57, 1-53.

Wendland, F., Kunkel, R., Müller, U., Tetzlaff, B., 2008. Area – differentiated modelling of groundwater recharge rate for determining quantitative status of groundwater; Case Study: Federal State of Lower Saxony, Germany. In: Mikulič, Z., Andjelov, M. (Eds.) Groundwater modelling. Proceedings of invited lecturers of Symposium on groundwater flow and transport modelling, Ljubljana, Slovenia, 28-31 January 2008, 73-79.

Wu, L., 2014. Groundwater recharge modelling approach to identify climate change impacts using groundwater levels from Tärnsjö. TRITA-LWR Degree Project 14, 19.

Zendehboudi, S., Shafiei, A., Chatzis, I., Dusseault, M.B., 2012. Numerical simulation of free fall and controlled gravity drainage processes in porous media. J. Porous Media 15 (3), 211–232.

Zomlot, Z., Verbeiren, B., Huysmans, M., Batelaan, O., 2015. Spatial distribution of groundwater recharge and base flow: assessment of controlling factors. J. Hydrol. Reg. Stud. 4, 349–368.